arXiv:1412.0324v1 [astro-ph.SR] 1 Dec 2014

CCD Photometry of NGC 2482 and Five Previously Unobserved Open Star Clusters

Kevin Krisciunas,[1] Hektor Monteiro,[2] and Wilton Dias[2]

ABSTRACT

We present BV and $u'g'r'i'$ CCD photometry of the central region of NGC 2482. We also present $BVu'g'$ CCD photometry of five clusters that have been poorly studied in the past: Ruprecht 42, Ruprecht 51, Ruprecht 153, Ruprecht 154; and AH03 J0748−26.9, which to our knowledge has not been studied before. Using a global optimization technique that eliminates much of the subjectivity previously inherent in main sequence fitting studies, we obtain values of the distances, ages, and metallicities of the clusters, with robust estimates of the uncertainties of these fundamental parameters. Four of our clusters are less than ∼1.3 kpc beyond the Sun's distance from the Galactic Center and have essentially solar metallicity. The metallicities of those clusters more distant from the Galactic Center are consistent with a 0.3 dex step to lower [Fe/H] found in other studies.

Subject headings: Photometry - stellar

1. Introduction

One of the fundamental distance determination methods within the Milky Way Galaxy is the method of main sequence fitting. After several decades of work by hundreds (or thousands) of astronomers, we believe we know the absolute magnitudes of single stars of a given age and metallicity. Since some stars in clusters are actually unresolved binaries, we can account for a "leakage" of stars in a color-magnitude diagram (CMD) to brighter values. Still, if we know which objects are bona fide members of a cluster, there should be

[1]George P. and Cynthia Woods Mitchell Institute for Fundamental Physics & Astronomy, Texas A. & M. University, Department of Physics & Astronomy, 4242 TAMU, College Station, TX 77843; krisciunas@physics.tamu.edu

[2]UNIFEI, IFQ - Instituto de Física e Química, Universidad Federal de Itajubá, Itajubá MG, Brazil; hektor.monteiro@gmail.com, wiltonsdias@yahoo.com.br

a sharper blue edge to the main sequence. Blue stragglers and stars along the same line of sight at other distances contribute to some raggedness of the blue edge. The bottom line is that we can determine the distances of clusters relative to the Hyades, whose distance we know from the moving cluster method (Hanson 1975) or, better still, from HIPPARCOS parallaxes (Perryman et al. 1998). Thus, we can determine the distances to the clusters using broad band photometry. As always, reddening can be problematic.

It is our assumption that stars in a cluster are born at about the same time and all have about the same composition. We are therefore intrigued by the recent finding that some *globular* clusters show evidence of two, or even three, main sequences (Milone et al. 2012; Piotto et al. 2007). To our knowledge there is no known open cluster that shows clear evidence of multiple stages of star formation.

Since the publication of the catalogue of open clusters of Alter, Ruprecht, & Vanýsek (1958) and its Supplements, the number of clusters has risen from 945 to more than 2000 (Dias et al. 2002).[3] Oliveira et al. (2013) point out that fewer than 10 percent of 2174 catalogued open clusters have their metallicity determined in the literature.

In this paper we present Johnson BV photometry and photometry using filters of the Sloan Digital Sky Survey (Fukugita et al. 1996). We have selected six clusters that have been poorly studied and one that, to our knowledge, has no published optical or near-IR photometry. We apply to the data the cross-entropy technique, first introduced by Rubinstein (1999), with the objective of estimating probabilities of rare events in complex stochastic networks, as previously done by Monteiro, Dias, & Caetano (2010), Oliveira et al. (2013), and references therein. The analysis uses a weighted likelihood criterion to define the goodness of fit and global optimization (i.e. cross-entropy) to find the best fit isochrones. For each cluster we derive the distance, age, $B-V$ color excess, and metallicity. For four clusters with moderate color excess we also derive $\mathrm{R}_V = \mathrm{A}_V/\mathrm{E}(B-V)$, which we set as a free parameter.

The clusters studied make a relevant contribution towards the establishement of a large sample of objects that have fundamental parameters, if not the observational data itself, determined in a homogenous way. Such a sample can be important in studies of Galactic structure and evolution.

In this paper we adopt a solar metallicity of $\mathrm{Z} = 0.019$, the value adopted for the set of isochrones of Marigo et al. (2008), which we use. The isochrone set of Marigo et al. (2008) was chosen because of its widespread use in the literature as well as its ease of use and implementation in our code. We refer the reader to that work for details and dicussion of

[3]The Dias catalogue is available online at http://www.astro.iag.usp.br/ocdb/.

the assumptions made by the authors. The distance of the Sun from the Galactic Center is taken to be 8.0 kpc (Reid 1993).

2. Data Acquisition and Reduction

2.1. The Clusters

Basic information for the clusters observed is given in Table 1. Details of the images used for this paper are given in Table 5, in the Appendix. The Appendix also gives transformation equations from instrumental magnitudes and colors to standardized values, and the reduction coefficients assumed and derived.

NGC 2482 (originally designated H VII 10) was discovered by William Herschel on 20 November 1784 with his 19-inch diameter reflector of 20-ft focal length (Herschel 1786, on p. 496).[4] He described it as, "A very large cluster of scattered stars extremely rich and compressed, more than 15′ in diameter."

According to Dias et al. (2002) NGC 2482 has an *apparent* distance modulus of 10.93 mag (meaning that extinction has not been taken into account), a distance of 1343 pc, a color excess $E(B-V) = 0.093$ mag, an age of 400 Myr, and an iron abundance of [Fe/H] = +0.12 dex. This abundance value is based on CMT_1T_2 Washington broad-band photometry of three giant stars by Clariá & Lapasset (1983). More recently, Reddy, Giridhar, & Lambert (2013) determined the metallicity of one of those stars, star 9 in the list of Moffat & Vogt (1975, Table 18), to be [Fe/H] = -0.07 ± 0.04.

Moffat & Vogt (1975) provide V magnitudes, $B-V$ and $U-B$ colors of 41 stars in the direction of NGC 2482. Seventeen of the stars are designated non-members of the cluster. Five of the 41 stars are considerably to the west (up to 15′) of the center of the cluster, near BX Puppis; one of these has photometry consistent with it being a cluster member. Most of the stars are distributed over a triangular region about 14′ by 11′ by 12′ in angular size.

According to Twarog, Ashman, & Anthony-Twarog (1997), "The [color-magnitude diagram] of Moffat & Vogt (1975) is too ill-defined to permit a reliable distance determination. Using the DDO modulus adjusted for the Hyades distance, one gets a very uncertain $(m-M)$

[4] A further examination of the observational record (Steinicke 2013, private communication) indicates that William Herschel saw the cluster again on 3 June 1785. His son John Herschel saw it with his own 18.25-inch reflector of 20-ft focal length on 7 January 1831 (catalogued as h 474). John Herschel saw it again on 28 January 1837 at the Cape of Good Hope with the same telescope (catalogued as h 3106).

= 10.3." This corresponds to a distance of 1148 pc.

To our knowledge the only reference to AH03 J0748−26.9 is in the catalogue of clusters by Archinal & Hynes (2003). Ruprecht 42, 51, 153 and 154 are listed by Ruprecht (1966). References cited in that work provide more information. Prior to our observations and analysis presented here, we were aware of no published photographic photometry, photoelectric photometry, or CCD photometry of these five clusters.[5]

2.2. Details of the Imagery

The data presented in this paper were obtained by one of us (KK) at Las Campanas Observatory (LCO) using the 1-m Henrietta Swope telescope. Three second exposures of NGC 2482 were obtained in $BVgri$ on 6 January 2012 (UT), along with a 24 second u-band exposure. Longer BV exposures of 150 and 120 seconds, respectively, were taken on 21 December 2012 (UT). For the NGC 2482 images we used the central 1201 × 1201 pixels of the CCD chip then in use. The pixel scale is 0.435 arc seconds; the field size is 8.7 by 8.7 arc minutes.

The other clusters were observed from 31 December 2013 to 4 January 2014 (UT) using a new CCD camera having four 2K by 2K chips. We observed all targets with chip number 3, offsetting 300 arcsec north and east of the center of the four chip array. We found after the fact that the point spread function (PSF) is good for chip 3 for X and Y ranging from about 600 to 2048 pixels. Along the left and bottom of chip 3, furthest from the center of the camera field of view, the PSF contours can significantly deviate from circularity. This is particularly the case for B-band images. We derived positions and magnitudes for stars over the whole of chip 3, but for the analysis of the clusters we restricted ourselves to a subset of the area covered. Given the angular size of the clusters, this feature of the PSF actually did not come into play in a significant way. The pixel scale is the same, so these images are 14.8 by 14.8 arc minutes in size.

For these five clusters we typically took one exposure per filter at or near the limit of the shortest exposure possible (5 seconds), and one or two exposures that were much longer (up to 120 sec). This minimizes the number of saturated stars and expands the dynamic range of the photometry.

The data presented here were all obtained on photometric nights, though on some occasions the seeing was worse at the start of the night. We observed standards of Landolt

[5]However, see comments below concerning the catalogue of Kharchenko et al. (2013).

(1992) and Smith et al. (2002) on five or six occasions each night.

2.3. The Photometry

Not only is NGC 2482 a good candidate for modern analysis, but its brightest stars did not reach the non-linear response level or saturation level of the shortest exposures possible with the CCD camera installed on the Las Campanas 1-m Swope telescope through 2012. This cluster was previously studied by Moffat & Vogt (1975) using single channel photoelectric photometry. Our PSF photometry, obtained from images of 6 January 2012, is given in Table 2. We give V and r' magnitudes and four photometric colors.

The coordinates of the NGC 2482 stars in Table 2 were determined using CCMAP and CCTRAN in the IMCOORDS package of IRAF.[6] We used the X-Y pixel coordinates of 10 stars distributed over the whole field and the right ascensions and declinations from a Digital Sky Survey[7] image displayed with DS9 to obtain the transformation solution.

In Table 3 we show the correspondence of our ID's and those of Moffat & Vogt (1975). There are 17 single stars in common. With "Δ" in the sense "our aperture photometry *minus* that of Moffat & Vogt (1975)", we find $\langle\Delta\ (V)\rangle = +0.024$ mag, with a standard deviation of the distribution of $\pm$ 0.035. We find $\langle\Delta\ (B-V)\rangle = +0.001$ mag, with a standard deviation of the distribution of $\pm$ 0.024. The average difference of our estimated $U-B$ colors compared to those of Moffat & Vogt (1975) is -0.033 mag, with a standard deviation of the distribution of $\pm$ 0.056. Thus, within the errors, our photometry of the brighter stars is in statistical agreement with previously published values.

We note that two of the stars of Moffat & Vogt (1975) show close companions in our imagery. A combination of the photometry of our stars 241 and 239 is in reasonable agreement (within 0.04 mag) with their star 17. Combined photometry of our stars 220 and 218 is in reasonable agreement with data of their star number 20.

In Fig. 1 we show an r' vs. $g'-r'$ color magnitude diagram of NGC 2482. The V vs. $B-V$ CMD is the middle two panels of Fig. 2. 11 of our 114 stars are obvious non-cluster members. They are presumably red giants at other distances. The brightest star in the field (our star 166) is a bona fide giant in the cluster.

---

[6]IRAF is distributed by the National Optical Astronomy Observatory, which is operated by the Association of Universities for Research in Astronomy, Inc., under cooperative agreement with the National Science Foundation (NSF).

[7]http://archive.stsci.edu/cgi-bin/dss_form

As noted above, the other five clusters were observed with a new CCD camera using a larger chip, but with the same plate scale. For these clusters we obtained photometry of a total of 3871 stars that satisfied the S/N criteria. The coordinates of the stars (in decimal degrees, and pixel coordinates) and the derived UBV photometry can be obtained by the reader via this link: people.physics.tamu/krisciunas/clusters.tar, which also contains data for 114 stars of NGC 2482 derived from PSF photometry. In the final column of each of these files we flag the stars most likely to be cluster members (normalized probability greater than 50 percent).[8] The coordinates given in the files are basically for the purpose of identification, not for astrometric studies requiring extreme accuracy.

2.4. Aperture Photometry vs. PSF Photometry

It is customary in star cluster studies to rely primarily on PSF photometry. This makes sense, as most open clusters are found at low Galactic latitude. There can be thousands of stars in the field, resulting in severe challenges for aperture photometry. To obtain the instrumental PSF magnitudes of our stars, we used a stand alone version of DAOPHOT (Stetson 1987) and ALLSTAR.[9] It is straightforward to keep track of the pixel coordinates and instrumental magnitudes, and adjust those magnitudes to the equivalent values for a 1.0 second exposure. However, instead of using DAOMATCH and DAOMASTER, we wrote our own FORTRAN software to cross-correlate the frames taken in different filters. We used the following selection criteria. We were interested in stars observed in *all* filters, 18-σ (or more) above the sky level in the u-band, and 30-σ (or more) above the sky level in the other filters. These selection criteria had the effect of eliminating many stars that are very red in $u' - g'$ and much redder than the main sequence of each cluster studied.

We should mention that one particular advantage of PSF photometry is that we can exploit our knowledge of the PSF to obtain a higher signal to noise ratio (S/N) for faint stars. We can dig deeper into the image. This is not too relevant to this paper however, since we wanted photometry accurate to 0.06 mag or better, so we limited ourselves to relatively bright stars, where the turnoff point of an open cluster typically lies.

---

[8]We note that the normalized probabilities are not membership probabilities in the classical sense, from proper motion vectors and/or radial velocities. The cross-entropy method maximizes a likelihood measure for an *ensemble* of stars. Even stars with low likelihood as members contribute to the multi-parameter solution.

[9]We found useful a web document called "A primer for DAOPHOT II and ALLSTAR" by Bill Harris (April 2002) and further extended by Helmut Jerjen. See: www.mso.anu.au/∼jerjen/daophot.html

Aperture photometry has its own advantages. Providing that the software aperture radius is sufficiently large (for the LCO 1-m we find this to be typically 8 pixels), accurate photometry can be ensured on photometric nights even if the PSF is considerably non-circular. The IRAF package APPHOT subtracts the sky level using a settable annulus, and if one uses the *median* counts in that annulus, cosmic ray hits or the presence of other stars in the annulus have no effect on the results. We typically used a sky annulus ranging from 12 to 20 pixels. Thus, aperture photometry *can* be used in moderately crowded fields.

Using the CCDRED package in IRAF we bias-corrected our images using a nightly master bias frame, flattened and trimmed them. The quality of each night was evaluated with observations of standards of Landolt (1992) and Smith et al. (2002). For this we used the PHOTCAL package in IRAF. This gave us photometric zero points and color terms. (See Appendix A and Table 6.) If the standards were observed over a sufficiently wide range of air mass, we also derived the atmospheric extinction and reddening terms. We did this for each night using the instrumental magnitudes of the standards derived from aperture photometry *and* from PSF photometry. Not surprisingly, the color terms and atmospheric terms were the same, within the errors, using the two methods. The instrumental magnitudes from PSF photometry (adjusted to a 1 second exposure time) are typically 0.02 to 0.04 mag brighter than the instrumental magnitudes from aperture photometry using an 8 pixel radius aperture. The PSF magnitudes include light most or all of the wings of the profile. And so the photometric zero points for transformations like Eqn. 1 are different by such an amount. One would have to use a very large software aperture to include "all" of the flux for the aperture magnitudes, and this greatly increases the chances of including other stars in the aperture. Our motivation here was to have the most robust reduction parameters to convert the PSF magnitudes and colors to standardized values using simple AWK scripts operating on our text files of raw PSF data.

In Fig. 3 we show a finder chart of 114 stars of NGC 2482 that were brighter than 18-σ above the sky level in the u-band, and 30-σ above the sky level in the other filters. Given the field size in pixels, this amounts to one "bright" star, on average, for every 112 by 112 pixel square of the image. Surely, by avoiding obvious close pairs, the results of aperture photometry and PSF photometry should be comparable.

A comparison of photometry done with the two methods is shown in Fig. 4. Aperture photometry of stars fainter than $V \approx 13.2$ was obtained on 21 December 2012. All PSF photometry comes from 6 January 2012. We have also accounted for a systematic error of 78 msec in the shutter time of the older camera at the LCO 1-m telescope (Hamuy et al. 2006, Appendix A).

Fig. 4 shows that there are no significant trends in the differences of aperture and

PSF photometry of NGC 2482 down to $V \approx 15.7$. The scatter of the individual differences increases, as expected, at fainter magnitudes, but the data are consistent to 0.06 mag or better.

We note that if one's ultimate goal is to produce color-magnitude diagrams, the internal errors are smaller for the colors if one sets up the data reduction to produce one magnitude and multiple colors using transformations specified in the configuration file (e.g in FITPARAMS in IRAF). In our experience at Cerro Tololo and LCO we find that the RMS scatter of the photometry of the standards on a photometric night is typically ± 0.025 mag in V, and ± 0.015 to 0.020 mag for $B - V$ colors. (These uncertainties should be added in quadrature to the internal random errors of the program objects.) If one configures FITPARAMS and EVALFIT to produce B-band magnitudes directly, the RMS error might be ± 0.025 mag or more. If one *then* obtains the $B - V$ colors by subtracting V magnitudes from B magnitudes, simple statistics stipulates that we would obtain uncertainties of ± 0.035 mag or more, roughly twice the RMS scatter for the colors obtained the other way using the same instrumental magnitudes. This is not a critical issue for stellar photometry, but it is something one should consider.

3. Analysis and Discussion

The cross-entropy technique applied to the isochrone fits done in this work is described in detail in a series of papers. See Oliveira et al. (2013) and references therein. It eliminates much of the subjectivity inherent in open cluster fitting. Using UBV photometry, it simultaneously solves for the reddening, distance, age, and metallicity of a cluster using an estimation of membership likelihood as described by Dias et al. (2012). A new feature of the program implemented in this work is that if the color excess of a cluster is greater than some settable value (we chose 0.1 mag), a value of $R_V = A_V/E(B-V)$ is also derived. Otherwise, $R_V = 3.1$ is assumed. The multi-parameter space considered is as follows: 1) log (age in years) from 6.60 to 10.15 in steps of 0.05; 2) 1 to 10,000 pc in distance; 3) $E(B-V)$ from 0.0 to 3.0 mag; 4) metallicity from 0.0001 to 0.03 in steps of 0.05 in log Z; and 5) R_V from 2.0 to 6.0. From a detailed analysis of nine well studied open clusters Oliveira et al. (2013) show that their technique works well.

Since the determination of the age of the cluster depends most critically on the hottest main sequence stars, those just past the turnoff point, and the red giants of the cluster, the lower main sequence stars are not critical but do help in constraining the general shape of the main sequence, especially with the U-band data. As a result, we may either set a limit on the faintest stars to consider, or let the program eliminate from consideration the stars

fainter than the maximum of a histogram of the V-band magnitudes, so as to have a sample reasonably complete to some brightness level. An extra piece of information we have on each star is its angular distance from the cluster center. If the images are sufficiently big to cover the whole extent of the cluster, the program can derive the most likely location of the center from the peak of a density map obtained with a Gaussian kernel of predefined width. One of the few arbitrary (but settable) parameters is the assumed fraction of unresolved binaries. With one exception we adopted 50 percent for this fraction. For NGC 2482 we adopted 40 percent for this fraction, as we found that it slightly improved the likelihood measure of our solution. Then, using a Salpeter (1955) mass function, we performed Monte Carlo simulations to pick at random the particulars of the companions. Carrying out a number of runs (typically 50) gives us the uncertainties of our derived parameters. Which stars are assigned binary status varies from run to run. Finally, in crowded fields with many giant star interlopers, some additional cuts by hand might be necessary on the basis of angular distance from the cluster center, the colors of the stars in the field and other data.

Concerning the reality of our targets being bona fide clusters, two of our targets (Ruprecht 153 and 154) were problematic, owing in part to the distribution of non-cluster stars in the field. This is a limitation of our method. For very crowded fields our procedure may fail to assign low weights to non-member stars solely on the basis of photometric data. In Fig. 5 we show a comparison of the density maps of the six clusters. For Ruprecht 153 we used a Gaussian kernel with $\sigma = 2.5'$. For the other clusters we used a kernal of $1'$.

For Ruprecht 154 we ran 100 iterations of the bootstrap procedure in order to sample better the distribution of solutions. The results show a clear double peaked distribution for the ages and non-Gaussian distributions for distance and reddening. The results are shown in Fig. 6, where we also present a 2D histogram in age versus distance showing that in this parameter space there are two well defined solutions with distinct ages and slightly different distances. The solution of lower age and distance seems to be the most probable, which is what we adopt. However, the results can be alternatively interpreted as two superimposed populations. Due to the small number of stars that have high likelihood of being cluster members, the results seem to be inconclusive for Ruprecht 154, since we can not rule out the possibility of chance alignment in the plane of the sky. A visual inspection of the proper motion vectors for the fields of both Ruprect 153 and Ruprecht 154 seem consistent with the latter hypothesis. Given all these considerations we believe that Ruprecht 153 and 154 warrant further study, including detailed analysis using proper motions, to better define their fundamental parameters or even their open cluster status. This, however, is beyond the scope of the present paper.

Results for the clusters observed are to be found in Table 4. The six clusters studied

have distances ranging from 1194 pc (NGC 2482) to 5457 pc (Ruprecht 42). The range in age is from 63 Myr (AH03 J0748−26.9) to 2.2 Gyr (Ruprecht 154). The weighted mean value of R_V for four clusters with moderate reddening is 3.06 ± 0.22, typical for "normal" Milky Way dust with $R_V = 3.1$ (Cardelli, Clayton, & Mathis 1989). In the final column of Table 4 we give the usual metallicity parameter [Fe/H] = log (Z/0.019).

Color-color diagrams and color-magnitude diagrams of the five clusters observed in December, 2013, and January, 2014, are shown in Figs. 7 through 11.

We have run the cross-entropy code on the PSF photometry *and* the aperture photometry of NGC 2482.[10] Using PSF photometry we obtain an age of 447 Myr, a distance of 1194 pc, $E(B-V) = 0.094$, and Z = 0.015. Using aperture photometry we obtain an age of 371 Myr, a distance of 1349 pc, $E(B-V) = 0.086$, and Z = 0.022. Given the uncertainties of the results given in Table 4, the corresponding differences are not statistically significant. The reader is free to average our two solutions for this cluster. We note that our value of [Fe/H] $= -0.10^{+0.13}_{-0.18}$ from PSF photometry is in excellent agreement with the value -0.07 ± 0.04 from spectroscopy of one giant in the cluster by Reddy, Giridhar, & Lambert (2013).

It is known that there is a decrease of metallicity with increasing distance from the Galactic Center. Many authors, such as Ryu & Lee (2011), fit a straight line to the data, obtaining a gradient of [Fe/H] amounting to −0.076 dex per kpc. Other authors show that it is more sensible to adopt a step function in the metallicity (Twarog, Ashman, & Anthony-Twarog 1997; Lépine et al. 2011). The metallicity is essentially constant, and comparable to that of the Sun, out to ∼1 kpc beyond the Sun's distance from the Galactic Center, then drops to [Fe/H] ≈ −0.30 beyond that. In Fig. 12 we show that our results are consistent with such a step function.

In Fig. 13 we present a plot of the positions of several hundred clusters from the catalogue of Dias et al. (2002) (those with the X-Y range shown), and our six clusters. We have coded the points by colors corresponding to the range of age in log t (in years). All of our clusters are situated in the Orion spur of the Galaxy, or in the Perseus arm; see Fig. 16 of Churchwell, et al. (2009). We note that of 1985 clusters in the catalogue of Dias et al. (2002) with ages specified, 80.6 percent have Galactic Z distances between −200 and +150 pc with respect to the Sun. There are only 21 clusters with |Z|> 1000 pc in the catalogue. The

[10]To provide a robust test of the consistency of the two data reduction methods, we ran the cross-entropy code on the *exact same* sample of 92 stars. Those identified by DAOPHOT included some stars close to the edges of the chip and obvious close pairs. Many stars selected by eye for aperture photometry from the longer and shorter V-band exposures are quite red and failed the 18-σ S/N criterion in the u-band for PSF photometry.

complex picture shown in Fig. 13 arises in part because we did not carry out any analysis of subsets of the Dias catalogue according to Galactic Cartesian coordinates.

Since we are interested in open clusters for distance determinations, we note that for our six clusters we obtain a mean *relative* uncertainty of distance of 8.8 percent. This corresponds to an uncertainty in the distance modulus of ± 0.183 mag. This may be compared to $\sigma_V = \pm 0.159$ mag from 649 fundamental mode Cepheids in the Large Magellanic Cloud and $\sigma_V = \pm 0.257$ mag from 466 fundamental mode Cepheids in the Small Magellanic Cloud (Udalski et al. 1999, Table 1). The intrinsic scatter of the absolute magnitudes of RR Lyrae stars is ± 0.24 mag or less (Layden et al. 1996). Type Ia supernovae at maximum light in the near-infrared are almost perfect standard candles. We know their absolute magnitudes to ± 0.15 mag or better (Krisciunas 2012).

It is also important to make a few points about the error estimates in this work, especially regarding the accuracy and precision of the method. It was shown by Monteiro, Dias, & Caetano (2010) that the method is accurate when evaluated against a synthetic cluster so that we have complete knowledge of the parameters used. This of course is not the case for real clusters where we have no "true" value to compare the fit results to. In this context our error estimates can be said to be precise, given the size of the errors relative to the parameters determined. However, this is completely dependent on the characteristics of the data used. So for a dataset that has many stars with low contamination, or contamination that can be removed easily, we will have very precise results, that is, with small error. The errors we quote are related to the precision of the *fit*. In other words, for a given dataset and likelihood function, weights, and isochrone grid assumptions used, the errors quoted are the standard deviations of the distribution of solutions obtained from the bootstrap procedure.

As we were finishing this paper we learned of the catalogue of 3006 bona fide objects of Kharchenko et al. (2013), which contains entries for five of our six clusters: NGC 2482, Ruprecht 42, 51, 153, and 154. Their parameters for NGC 2482 are in agreement with our results thanks to previously published optical data by Moffat & Vogt (1975), but their parameters for the four Ruprecht clusters differ considerably from ours. For example, their entry for Ruprecht 154 gives a color excess $\mathrm{E}(B-V) = 0.781$ mag and an age of 14 Myr, while we obtain 0.087 mag and 2.2 Gyr, respectively, for the same cluster! Also, note how different is the isochrone corresponding to their value of the cluster age of Ruprecht 42 in Fig. 8.

Kharchenko et al. (2013) used PPMXL,[11] a catalog of positions, proper motions, optical

[11]http://irsa.ipac.caltech.edu/Missions/ppmxl.html

photometry, and near-IR photometry from the Two Micron All-sky Survey.[12] While Dias et al. (2012) have demonstrated that 2MASS photometry alone *can* lead to sensible results for some clusters, we find that a near-IR color-magnitude of 2MASS data of AH03 J0748−26.9 reveals no obvious main sequence, while our optical data clearly shows one. An attempt by us to fit the near-IR data of Ruprecht 154 also yielded no scientific fruit. We surmise that the photometric depth and accuracy of the 2MASS catalogue alone is not enough to resolve the main sequence and turnoff point of many clusters superimposed on crowded fields. Since Kharchenko et al. (2013) have based some of their catalogue entries on 2MASS data, without the use of optical photometry, the reader should treat some of the individual entries of their catalogue with caution.

4. Conclusions

We have presented broad band photometry of six Galactic open clusters, four of which were poorly studied (no optical CCD photometry) and one that has never been studied before. Using the cross-entropy method applied to the fitting of theoretical isochrones to photometric data as detailed by Monteiro, Dias, & Caetano (2010), for each cluster we have derived the age, distance, reddening, and metallicity, with robust error bars.

Four of our six clusters, those less than 1.3 kpc beyond the Sun's distance from the Galactic center, have metallicity slightly greater than that of the Sun ($\langle Z \rangle = 0.022 \pm 0.002$), while two of our clusters beyond this distance have lower than solar metallicity ($\langle Z \rangle = 0.012 \pm 0.003$). The individual values, converted to [Fe/H] in the usual way, are consistent with the step function found by Twarog, Ashman, & Anthony-Twarog (1997), and Lépine et al. (2011).

As mentioned by Oliveira et al. (2013), only about 10 percent of 2174 catalogued open clusters have published values of metallicity. Many of these are obtained from spectroscopy, which is the preferred method. However, observationaly, this is a costly endeavor and alternatives that allow for the determination of the metallicity for a large number of clusters are desirable. In this context, values determined from photometry as done in this work can have an important impact in the research fields that use metallicity as a tool. Efforts to complete the catalog may lie far in the future and may require a large scale Galactic plane survey, something that may soon be possible using modern instruments and techniques. The tools and procedures such as those used in this work will surely be important in that scenario.

[12]http://www.ipac.caltech.edu/2mass/releases/allsky/index.html; see also Skrutskie et al. (2006).

We suggest three worthwhile follow up endeavors: 1) Obtain high resolution spectra of several stars brighter than $V \approx 14$ in NGC 2482 that are ≈ 0.3 mag redder or bluer than the median colors of other presumed main sequence stars of comparable brightness. This will shed light on the issue of unresolved binaries. 2) A much bigger project is to obtain accurate proper motions of our six clusters in order to eliminate obvious non-cluster stars. Since the mean proper motions of these clusters are only a few milliarcsec per year, this will be a challenge. 3) Carry out a detailed analysis of the spatial and kinematical structure of the Galaxy. This would be, in effect, a four dimensional version of our Fig. 13 (three spatial dimensions and one of time).

We thank Woody Sullivan and Wolfgang Steinicke for their intimate knowledge of William Herschel's observations. We thank Lucas Macri for installing a stand alone version of DAOPHOT and ALLSTAR, and for useful references. Wenlong Yuan and Alejandro Lorenzo helped with data analysis. We thank an anonymous referee for useful suggestions. We particularly thank Mark Phillips for the opportunity to take the imagery presented here while observing for the Carnegie Supernova Project. The observations presented here were a backup program for times when there were no reasonably bright supernovae high in the sky.

H. Monteiro would like to thank FAPEMIG for the grant CEX-PPM-00235-12 and Cnpq grant 306632/2013-6.

A. Further Details of the Imagery and Data Reduction

In Table 5 we give the exposure times and seeing (in pixels) of the imagery used for this project. Table 6 gives the adopted (or derived) atmospheric extinction and reddening parameters used for the data reduction along with the derived color terms, photometric zeropoints, and the RMS uncertainties of the nightly fits. The camera used for the 2012 imagery of NGC 2482 was replaced prior to the December 2013/January 2014 observing run. One can see that the color terms obtained from the observations of standard stars are consistent from night to night for observations with the same camera.

Typical transformations from the instrumental magnitudes to standardized ones are as follows:

$$V \; = \; v \; - \; k_v X_v \; + \; \epsilon_V (b - v) \; + \; \zeta_V \; ; \tag{A1}$$

$$B \; = \; b \; - \; k_b X_b \; + \; \epsilon_B (b - v) \; + \; \zeta_B \; ; \tag{A2}$$

$$u' - g' \; = \; \mu_{ug} (u - g) \; - \; k_{ug} \bar{X}_{ug} \; + \; \zeta_{ug} \; . \tag{A3}$$

Comparable transformation equations can be written to produce r', $g' - r'$ and $r' - i'$. The values on the right hand sides (u, b, v, g) are instrumental magnitudes. k values are atmospheric extinction or reddening terms. X (or $\bar{X}$) is the air mass value for an observation in a given filter (or the average of the air mass values for two filters), ϵ's and μ's are color terms, and ζ's are photometric zero points. The values on the left hand sides are standardized V and B magnitudes in the Landolt (1992) system. $u' - g'$ is the color in the Sloan "primed" system of Smith et al. (2002).

A transformation of our measured $u' - g'$ colors to $U - B$ colors can be obtained from the values for the standards observed on a particular night given by Landolt (1992) and Smith et al. (2002). For example, given the standards used on 6 January 2012, we obtain::

$$(U - B)_{Landolt} \; = \; (0.792 \pm 0.018) \; (u' - g') \; - \; (0.877 \pm 0.031) \; . \tag{A4}$$

REFERENCES

Alter, G., Ruprecht, J., & Vanýsek 1958, Catalogue of Star Clusters and Associations, Publishing House of the Czechoslovak Academy of Sciences, Prague

Archinal, B., & Hynes, S. 2003, Star Clusters, Richmond, Virginia: Willmann-Bell

Cardelli, J. A., Clayton, G. C., & Mathis, J. S. 1989, ApJ, 345, 245

Churchwell, E., Babler, B. L., Meade, M. R., et al. 2009, PASP, 121, 213

Clariá, J. J., & Lapasset, E. 1983, J. Astrophys. Astr. 4, 117

Dias, W. S., Alessi, B. S., Motinho, A., & Lépine, J. R. D. 2002, A&A, 389, 871

Dias, W. S., Monteiro, H., Caetano, T. C., & Oliveira, A. F. 2012, A&A, 539, A125

Fukugita, M., Ichikawa, T., Gunn, J. E., Doi, M., Shimasaku, K., & Schneider, D. P. 1996, AJ, 111, 1748

Hamuy, M., Folatelli, G., Morrell, N. I., et al. 2006, PASP, 118, 2

Hanson, R. B. 1975, AJ, 80, 379

Herschel, W. 1786, Phil. Trans. Royal Soc. London, 76, 457

Kharchenko, N. V., Piskunov, A. E., Schilbach, E. et al., 2013, A&A, 558, 53

Krisciunas, K. 2012, J. of the Amer. Assoc. of Variable Star Observers, 40, 334

Landolt, A. U. 1992, AJ, 104, 372

Layden, A. C., Hanson, R. B., Hawley, S. L., Klemola, A. R., & Hanley, C. J. 1996, AJ, 112, 2110

Lépine, J. R. D., Cruz, P., Scarano, S., Jr., et al. 2011, MNRAS, 417, 698

Marigo, P., Girardi, L., Bressan, A., Groenewegen, M. A. T., Silva, L., & Granato, G. L. 2008, A&A, 482, 883

Milone, A. P., Marino, A. F., Piotto, G., et al. 2012, ApJ, 745, 27

Moffat, A. F. J., & Vogt, N. 1975, A&AS, 20, 85

Monteiro, H., Dias, W. S., & Caetano, T. C. 2010, A&A, 516, A2

Oliveira, A. F., Monteiro, H., Dias, W. S., & Caetano, T. C. 2013 A&A, 557, A14

Perryman, M. A. C., Brown, A. G. A., Lebreton, Y., et al. 1998, A&A, 331, 81

Piotto, G., Bedin, L. R., Anderson, J., et al. 2007, ApJ, 661, L53

Reid, M. J. 1993, ARA&A, 31, 345

Reddy, A. B. S., Giridhar, S., & Lambert, D. L. 2013, MNRAS, 431, 3338

Rubinstein, R. 1999, Methodology and Computing in Applied Probability, 1, 127

Ruprecht, J. 1966, Bull. Astron. Inst. Czechoslovakia, 17, 33

Ryu, J., & Lee, G. 2011, J. Korean Astron. Soc., 44, 177

Salpeter, E. E. 1955, ApJ, 121, 161

Skrutskie, M. F., Cutri, R. M., Stiening, R., et al. 2006, AJ, 131, 1163

Stetson, P. B. 1987, PASP, 99, 191

Smith, J. A., Tucker, D. L., Kent, S., et al. 2002, AJ, 123, 2121

Twarog, B. A., Ashman, K. M., & Anthony-Twarog, B. J. 1997, AJ, 114, 2556

Udalski, A., Szymański, M., Kubiak, M., Pietrzyński, G., Soszyński, I., Woźniak, P., & Zebruń, K. 1999, Acta Astron. 49, 201

This preprint was prepared with the AAS LaTeX macros v5.2.

Table 1. Clusters Observed[a]

Cluster	RA	DEC	l	b	μ_{RA}	μ_{DEC}	Filters	N
AH03 J0748−26.9	7:48:40	−26:56:48	243.183	−0.606	...	...	$uBVg$	708
NGC 2482	7:55:12	−24:15:30	241.626	+2.035	−03.29 (0.17)	+03.29 (0.15)	$uBVgri$	114
Ruprecht 42	7:57:36	−25:55:00	243.326	+1.639	−02.67 (0.39)	+03.41 (0.05)	$uBVg$	958
Ruprecht 153	8:00:19	−30:17:00	247.360	−0.139	−02.40 (0.19)	−00.39 (0.35)	$uBVg$	586
Ruprecht 154	8:01:46	−44:25:00	259.581	−7.302	−05.16 (0.93)	+02.67 (0.75)	$uBVg$	461
Ruprecht 51	8:03:37	−30:39:00	248.048	+0.270	−02.81 (0.22)	+00.16 (0.28)	$uBVg$	1158

[a]For each cluster we give the RA and DEC for equinox J2000 of the nominal cluster center, the corresponding Galactic longitude and latitude (in degrees), the mean proper motion of the cluster in RA and DEC (milliarcsec per year), the filters used, and the number of stars identified by DAOPHOT that satisfied the apparent magnitude criteria (18-σ over sky in u and 30-σ over sky in the other filters).

Table 2. Photometry of NCG 2482 Central Region[a]

RA[b]	DEC[b]	V	$B-V$	$u'-g'$	r'	$g'-r'$	$r'-i'$	ID
7:54:56.64	−24:12:59.9	15.677 (0.034)	0.476 (0.057)	1.419 (0.078)	15.588 (0.046)	0.269 (0.046)	0.065 (0.042)	86
7:54:56.76	−24:15:52.9	15.058 (0.031)	0.613 (0.054)	1.235 (0.071)	14.926 (0.041)	0.342 (0.041)	0.136 (0.040)	174
7:54:56.76	−24:16:05.2	15.697 (0.042)	0.511 (0.062)	1.073 (0.072)	15.514 (0.039)	0.390 (0.039)	0.151 (0.039)	178
7:54:57.68	−24:11:54.3	12.819 (0.029)	0.258 (0.033)	1.217 (0.059)	12.848 (0.031)	−0.018 (0.031)	−0.066 (0.039)	52
7:54:58.37	−24:13:42.5	11.693 (0.024)	0.107 (0.024)	1.128 (0.058)	11.774 (0.030)	−0.146 (0.030)	−0.173 (0.033)	112
7:54:58.97	−24:16:00.8	11.228 (0.024)	0.082 (0.028)	1.118 (0.057)	11.308 (0.028)	−0.173 (0.028)	−0.177 (0.030)	177
7:54:59.14	−24:15:50.6	12.379 (0.024)	0.184 (0.026)	1.186 (0.056)	12.435 (0.029)	−0.075 (0.029)	−0.129 (0.030)	172
7:54:59.32	−24:12:10.8	15.154 (0.038)	0.718 (0.052)	1.580 (0.074)	14.900 (0.039)	0.535 (0.039)	0.237 (0.048)	60
7:54:59.39	−24:15:48.5	15.616 (0.035)	0.366 (0.052)	1.404 (0.068)	15.534 (0.040)	0.217 (0.040)	0.038 (0.045)	168
7:55:01.21	−24:11:17.3	15.030 (0.040)	0.595 (0.052)	1.190 (0.069)	14.871 (0.044)	0.354 (0.044)	0.132 (0.050)	32
7:55:01.25	−24:17:44.1	15.649 (0.037)	0.443 (0.053)	1.519 (0.077)	15.519 (0.037)	0.289 (0.037)	0.068 (0.046)	231
7:55:02.02	−24:18:15.0	13.934 (0.027)	0.426 (0.030)	1.102 (0.056)	13.847 (0.028)	0.238 (0.028)	0.031 (0.033)	251
7:55:02.15	−24:12:59.4	15.273 (0.039)	0.371 (0.048)	1.449 (0.071)	15.164 (0.043)	0.231 (0.043)	0.071 (0.044)	87
7:55:02.22	−24:13:41.5	13.429 (0.026)	0.412 (0.029)	1.363 (0.057)	13.414 (0.028)	0.147 (0.028)	−0.006 (0.034)	111
7:55:02.48	−24:16:44.6	14.570 (0.031)	0.512 (0.039)	1.146 (0.059)	14.437 (0.030)	0.321 (0.030)	0.100 (0.036)	203
7:55:03.00	−24:18:04.9	14.901 (0.030)	0.521 (0.039)	1.412 (0.062)	14.854 (0.035)	0.240 (0.035)	0.077 (0.041)	245
7:55:03.21	−24:14:11.7	13.706 (0.025)	1.332 (0.033)	2.833 (0.071)	13.229 (0.028)	1.088 (0.028)	0.486 (0.033)	120
7:55:03.98	−24:10:38.6	14.719 (0.036)	0.635 (0.046)	1.300 (0.066)	14.546 (0.038)	0.403 (0.038)	0.133 (0.046)	10
7:55:04.29	−24:18:19.0	15.363 (0.038)	0.374 (0.050)	1.396 (0.066)	15.385 (0.039)	0.115 (0.039)	0.081 (0.043)	255
7:55:04.47	−24:16:51.0	10.756 (0.022)	0.127 (0.022)	1.122 (0.054)	10.835 (0.023)	−0.124 (0.023)	−0.156 (0.029)	206
7:55:05.18	−24:15:15.7	12.968 (0.022)	0.184 (0.025)	0.954 (0.055)	13.002 (0.023)	−0.013 (0.023)	−0.112 (0.029)	154
7:55:05.28	−24:17:06.4	14.072 (0.027)	0.467 (0.031)	1.147 (0.058)	13.939 (0.028)	0.311 (0.028)	0.086 (0.034)	212
7:55:05.34	−24:16:39.2	12.037 (0.022)	0.475 (0.023)	1.174 (0.054)	11.926 (0.024)	0.285 (0.024)	0.055 (0.032)	200
7:55:05.48	−24:16:34.9	15.288 (0.036)	0.662 (0.051)	1.489 (0.072)	15.013 (0.034)	0.519 (0.034)	0.180 (0.043)	196
7:55:05.56	−24:15:07.0	15.041 (0.026)	0.428 (0.038)	1.437 (0.062)	15.013 (0.033)	0.162 (0.033)	0.087 (0.047)	149
7:55:06.22	−24:17:54.2	14.965 (0.033)	0.672 (0.042)	1.320 (0.062)	14.748 (0.039)	0.486 (0.039)	0.183 (0.047)	238
7:55:06.34	−24:11:21.6	13.898 (0.029)	0.587 (0.034)	1.414 (0.062)	13.755 (0.036)	0.369 (0.036)	0.121 (0.043)	37
7:55:06.99	−24:18:58.5	14.668 (0.031)	0.510 (0.040)	1.212 (0.061)	14.567 (0.038)	0.340 (0.038)	0.121 (0.038)	280
7:55:07.12	−24:18:27.3	14.529 (0.032)	0.544 (0.042)	1.190 (0.062)	14.331 (0.032)	0.410 (0.032)	0.107 (0.041)	261
7:55:07.57	−24:18:42.2	12.963 (0.026)	0.281 (0.027)	1.192 (0.055)	12.984 (0.032)	0.057 (0.032)	−0.020 (0.038)	272
7:55:08.30	−24:15:10.2	12.045 (0.023)	0.152 (0.022)	0.405 (0.054)	12.095 (0.033)	−0.060 (0.033)	−0.078 (0.043)	150
7:55:08.47	−24:15:48.7	15.466 (0.037)	0.538 (0.050)	1.371 (0.073)	15.341 (0.041)	0.355 (0.041)	0.159 (0.043)	171
7:55:08.73	−24:14:45.1	15.418 (0.031)	0.510 (0.046)	1.438 (0.073)	15.269 (0.035)	0.332 (0.035)	0.103 (0.034)	138
7:55:08.76	−24:17:45.7	12.512 (0.025)	0.357 (0.026)	1.208 (0.054)	12.489 (0.028)	0.129 (0.028)	0.003 (0.034)	232
7:55:09.10	−24:15:01.5	14.407 (0.094)	1.253 (0.130)	2.014 (0.144)	14.040 (0.168)	0.826 (0.168)	0.361 (0.168)	146

Table 2—Continued

RA[b]	DEC[b]	V	$B-V$	$u'-g'$	r'	$g'-r'$	$r'-i'$	ID
7:55:09.71	−24:18:16.5	12.856 (0.027)	0.223 (0.027)	1.269 (0.055)	12.884 (0.032)	−0.003 (0.032)	−0.042 (0.034)	253
7:55:09.98	−24:12:06.2	11.620 (0.028)	1.688 (0.029)	3.515 (0.062)	10.976 (0.033)	1.418 (0.033)	0.627 (0.031)	57
7:55:10.25	−24:11:36.4	12.364 (0.031)	0.162 (0.033)	1.210 (0.057)	12.427 (0.030)	−0.078 (0.030)	−0.099 (0.037)	46
7:55:10.58	−24:16:21.9	11.121 (0.021)	0.122 (0.020)	1.160 (0.053)	11.216 (0.025)	−0.145 (0.025)	−0.139 (0.027)	189
7:55:10.89	−24:17:37.3	15.453 (0.040)	0.456 (0.050)	1.394 (0.071)	15.405 (0.041)	0.196 (0.041)	0.115 (0.037)	227
7:55:11.10	−24:17:48.6	11.855 (0.025)	0.126 (0.026)	1.154 (0.054)	11.953 (0.029)	−0.135 (0.029)	−0.115 (0.033)	234
7:55:11.53	−24:15:11.1	13.739 (0.022)	0.437 (0.025)	1.125 (0.055)	13.672 (0.025)	0.201 (0.025)	0.032 (0.030)	153
7:55:11.54	−24:14:35.6	14.548 (0.030)	0.568 (0.037)	1.462 (0.061)	14.394 (0.031)	0.387 (0.031)	0.230 (0.032)	133
7:55:11.59	−24:11:01.9	13.400 (0.032)	0.069 (0.034)	0.578 (0.059)	13.440 (0.036)	−0.096 (0.036)	−0.121 (0.045)	23
7:55:11.61	−24:11:48.2	14.252 (0.030)	0.634 (0.040)	1.212 (0.060)	14.083 (0.033)	0.446 (0.033)	0.133 (0.036)	50
7:55:11.74	−24:14:36.0	15.688 (0.038)	0.588 (0.060)	1.127 (0.066)	15.527 (0.036)	0.435 (0.036)	0.116 (0.042)	135
7:55:11.74	−24:17:42.5	15.108 (0.036)	0.585 (0.045)	1.457 (0.066)	14.907 (0.042)	0.438 (0.042)	0.211 (0.050)	230
7:55:11.82	−24:13:38.7	10.646 (0.022)	0.122 (0.020)	1.181 (0.053)	10.739 (0.020)	−0.141 (0.020)	−0.111 (0.022)	108
7:55:11.84	−24:15:17.8	14.587 (0.028)	0.600 (0.035)	1.270 (0.061)	14.428 (0.036)	0.374 (0.036)	0.136 (0.039)	156
7:55:11.94	−24:17:31.6	13.731 (0.029)	0.513 (0.032)	1.188 (0.056)	13.610 (0.031)	0.310 (0.031)	0.150 (0.041)	222
7:55:12.05	−24:15:23.6	13.251 (0.022)	0.423 (0.023)	1.086 (0.055)	13.152 (0.027)	0.238 (0.027)	0.071 (0.026)	157
7:55:13.02	−24:12:08.1	12.758 (0.026)	1.089 (0.028)	2.252 (0.059)	12.407 (0.029)	0.835 (0.029)	0.343 (0.034)	59
7:55:13.57	−24:15:41.6	10.220 (0.022)	1.102 (0.022)	2.312 (0.054)	9.972 (0.021)	0.687 (0.025)	0.299 (0.016)	166
7:55:13.82	−24:16:03.7	12.877 (0.025)	0.267 (0.025)	1.204 (0.055)	12.891 (0.029)	0.031 (0.029)	−0.003 (0.034)	179
7:55:13.92	−24:14:35.4	15.431 (0.031)	0.777 (0.048)	1.412 (0.075)	15.218 (0.038)	0.559 (0.038)	0.224 (0.043)	134
7:55:14.15	−24:18:47.9	15.354 (0.045)	0.798 (0.063)	1.548 (0.078)	15.126 (0.058)	0.602 (0.058)	0.231 (0.063)	275
7:55:15.36	−24:12:28.8	14.699 (0.035)	0.442 (0.042)	1.384 (0.063)	14.727 (0.030)	0.118 (0.030)	0.092 (0.042)	73
7:55:15.80	−24:13:19.1	11.262 (0.021)	0.099 (0.021)	1.106 (0.054)	11.372 (0.021)	−0.152 (0.021)	−0.121 (0.031)	94
7:55:15.87	−24:17:09.9	14.329 (0.028)	0.319 (0.033)	1.244 (0.058)	14.323 (0.033)	0.133 (0.033)	0.019 (0.038)	214
7:55:15.90	−24:12:11.0	13.515 (0.025)	0.535 (0.030)	1.161 (0.057)	13.390 (0.028)	0.332 (0.028)	0.102 (0.033)	62
7:55:16.15	−24:16:34.1	11.410 (0.024)	1.333 (0.027)	2.973 (0.057)	10.954 (0.027)	1.054 (0.027)	0.414 (0.027)	197
7:55:16.77	−24:12:42.1	15.294 (0.036)	0.675 (0.048)	1.376 (0.070)	15.047 (0.043)	0.590 (0.043)	0.246 (0.048)	78
7:55:16.90	−24:12:12.9	12.525 (0.025)	0.195 (0.025)	1.209 (0.055)	12.580 (0.030)	−0.057 (0.030)	−0.108 (0.040)	66
7:55:17.30	−24:12:09.5	12.752 (0.025)	0.434 (0.030)	1.331 (0.055)	12.663 (0.030)	0.238 (0.030)	0.048 (0.031)	61
7:55:17.52	−24:11:22.1	15.211 (0.041)	0.700 (0.050)	1.206 (0.065)	15.025 (0.039)	0.485 (0.039)	0.186 (0.051)	38
7:55:17.93	−24:16:18.0	12.670 (0.023)	0.246 (0.024)	1.108 (0.055)	12.668 (0.029)	0.056 (0.029)	−0.024 (0.029)	187
7:55:18.75	−24:17:41.0	11.425 (0.026)	0.087 (0.027)	1.138 (0.058)	11.519 (0.035)	−0.143 (0.035)	−0.161 (0.045)	229
7:55:19.42	−24:12:55.9	11.848 (0.024)	1.167 (0.028)	2.646 (0.056)	11.419 (0.027)	0.949 (0.027)	0.353 (0.032)	85
7:55:19.46	−24:14:49.4	11.754 (0.021)	0.242 (0.021)	1.329 (0.054)	11.748 (0.022)	0.034 (0.022)	−0.097 (0.021)	143
7:55:19.46	−24:17:56.6	11.881 (0.028)	1.370 (0.031)	2.720 (0.061)	11.400 (0.040)	1.110 (0.040)	0.468 (0.048)	242

Table 2—Continued

RA[b]	DEC[b]	V	$B-V$	$u'-g'$	r'	$g'-r'$	$r'-i'$	ID
7:55:20.12	−24:10:55.7	11.592 (0.030)	0.198 (0.035)	1.267 (0.056)	11.648 (0.034)	−0.044 (0.034)	−0.084 (0.044)	19
7:55:20.59	−24:13:28.1	13.391 (0.022)	1.527 (0.029)	3.067 (0.065)	12.862 (0.027)	1.238 (0.027)	0.597 (0.028)	103
7:55:20.63	−24:18:36.0	15.323 (0.035)	0.445 (0.046)	1.363 (0.072)	15.257 (0.051)	0.238 (0.051)	0.074 (0.064)	269
7:55:20.73	−24:14:44.1	12.682 (0.022)	0.163 (0.022)	1.218 (0.054)	12.720 (0.025)	−0.065 (0.025)	−0.114 (0.023)	139
7:55:20.78	−24:17:52.1	13.501 (0.029)	0.306 (0.032)	1.280 (0.062)	13.459 (0.042)	0.120 (0.042)	0.001 (0.049)	239
7:55:20.92	−24:17:55.1	11.926 (0.028)	0.246 (0.030)	1.179 (0.060)	11.924 (0.040)	0.052 (0.040)	−0.043 (0.046)	241
7:55:20.98	−24:17:24.4	12.287 (0.024)	0.149 (0.026)	1.210 (0.058)	12.354 (0.034)	−0.098 (0.034)	−0.141 (0.040)	220
7:55:21.16	−24:17:20.9	15.130 (0.035)	0.649 (0.052)	1.316 (0.066)	14.926 (0.040)	0.514 (0.040)	0.233 (0.038)	218
7:55:21.87	−24:10:48.4	13.939 (0.031)	1.138 (0.045)	2.184 (0.067)	13.510 (0.043)	0.937 (0.043)	0.407 (0.051)	15
7:55:22.20	−24:10:45.9	14.338 (0.036)	0.552 (0.044)	1.179 (0.060)	14.189 (0.038)	0.357 (0.038)	0.095 (0.048)	13
7:55:22.34	−24:16:45.2	14.754 (0.030)	0.722 (0.043)	1.483 (0.063)	14.544 (0.035)	0.507 (0.035)	0.125 (0.038)	204
7:55:22.51	−24:18:16.7	12.585 (0.030)	0.480 (0.033)	1.134 (0.062)	12.463 (0.040)	0.309 (0.040)	0.072 (0.052)	256
7:55:22.70	−24:13:26.8	14.118 (0.026)	0.293 (0.033)	1.023 (0.057)	14.086 (0.028)	0.113 (0.028)	−0.004 (0.032)	102
7:55:23.06	−24:14:22.1	14.967 (0.032)	0.595 (0.041)	1.177 (0.062)	14.843 (0.033)	0.401 (0.033)	0.090 (0.036)	129
7:55:23.09	−24:10:58.4	13.123 (0.030)	0.184 (0.036)	0.691 (0.056)	13.157 (0.037)	−0.044 (0.037)	−0.072 (0.046)	21
7:55:23.11	−24:15:45.8	13.526 (0.024)	0.353 (0.026)	1.159 (0.057)	13.471 (0.030)	0.169 (0.030)	−0.016 (0.031)	170
7:55:23.43	−24:18:29.0	13.412 (0.031)	0.327 (0.037)	1.198 (0.063)	13.359 (0.042)	0.131 (0.042)	−0.003 (0.051)	265
7:55:24.00	−24:17:51.0	15.392 (0.036)	0.458 (0.048)	1.457 (0.068)	15.278 (0.044)	0.280 (0.044)	0.065 (0.051)	236
7:55:24.18	−24:14:51.3	12.229 (0.022)	0.212 (0.024)	1.210 (0.055)	12.224 (0.027)	0.032 (0.027)	−0.072 (0.029)	144
7:55:24.20	−24:18:40.2	14.951 (0.042)	0.682 (0.054)	1.280 (0.064)	14.726 (0.051)	0.534 (0.051)	0.195 (0.050)	273
7:55:24.20	−24:18:51.8	14.548 (0.039)	0.571 (0.047)	1.374 (0.069)	14.352 (0.045)	0.430 (0.045)	0.169 (0.051)	278
7:55:24.36	−24:17:33.3	15.027 (0.031)	0.625 (0.039)	1.203 (0.069)	14.900 (0.044)	0.363 (0.044)	0.155 (0.051)	224
7:55:24.48	−24:18:00.1	12.755 (0.047)	0.582 (0.061)	1.245 (0.080)	12.618 (0.096)	0.386 (0.096)	0.010 (0.101)	244
7:55:24.91	−24:16:50.7	11.425 (0.025)	0.110 (0.026)	1.180 (0.058)	11.462 (0.032)	−0.084 (0.032)	−0.133 (0.038)	208
7:55:25.25	−24:10:34.3	14.650 (0.032)	0.612 (0.045)	1.273 (0.061)	14.472 (0.039)	0.418 (0.039)	0.189 (0.049)	9
7:55:25.54	−24:10:34.1	14.772 (0.040)	0.529 (0.048)	1.174 (0.064)	14.604 (0.047)	0.335 (0.047)	0.131 (0.052)	8
7:55:25.73	−24:15:42.6	15.285 (0.030)	0.781 (0.048)	1.432 (0.066)	15.103 (0.040)	0.531 (0.040)	0.191 (0.044)	167
7:55:26.16	−24:12:42.7	14.575 (0.031)	1.242 (0.051)	2.242 (0.073)	14.127 (0.037)	1.001 (0.037)	0.416 (0.038)	79
7:55:26.81	−24:18:57.2	11.435 (0.037)	0.102 (0.043)	0.642 (0.065)	11.439 (0.047)	−0.038 (0.047)	−0.140 (0.060)	283
7:55:26.86	−24:12:15.2	15.404 (0.034)	0.691 (0.053)	1.399 (0.068)	15.167 (0.046)	0.475 (0.046)	0.147 (0.051)	68
7:55:27.59	−24:13:30.5	14.556 (0.030)	0.475 (0.042)	1.068 (0.060)	14.403 (0.038)	0.299 (0.038)	0.101 (0.041)	104
7:55:27.61	−24:14:44.4	13.044 (0.024)	0.267 (0.028)	1.237 (0.056)	13.003 (0.032)	0.088 (0.032)	−0.083 (0.033)	140
7:55:27.82	−24:11:55.0	12.890 (0.027)	0.331 (0.037)	1.138 (0.058)	12.807 (0.040)	0.169 (0.040)	0.023 (0.041)	53
7:55:28.14	−24:12:36.6	15.513 (0.036)	0.605 (0.052)	1.364 (0.074)	15.287 (0.050)	0.401 (0.050)	0.154 (0.052)	77
7:55:28.30	−24:16:15.0	13.285 (0.025)	0.440 (0.028)	0.903 (0.057)	13.137 (0.030)	0.291 (0.030)	0.072 (0.037)	185

Table 2—Continued

RA[b]	DEC[b]	V	$B-V$	$u'-g'$	r'	$g'-r'$	$r'-i'$	ID
7:55:29.15	−24:14:57.4	13.493 (0.026)	0.474 (0.034)	1.187 (0.058)	13.344 (0.039)	0.323 (0.039)	0.030 (0.042)	145
7:55:29.39	−24:14:22.6	13.008 (0.023)	0.265 (0.027)	1.194 (0.057)	12.964 (0.032)	0.093 (0.032)	−0.104 (0.034)	130
7:55:29.66	−24:17:01.8	13.312 (0.030)	0.408 (0.033)	1.180 (0.059)	13.194 (0.035)	0.249 (0.035)	0.024 (0.045)	211
7:55:29.78	−24:12:01.1	13.115 (0.024)	0.280 (0.037)	1.049 (0.056)	13.054 (0.041)	0.123 (0.041)	−0.006 (0.040)	56
7:55:31.14	−24:10:29.9	14.105 (0.030)	0.694 (0.044)	1.351 (0.060)	13.874 (0.048)	0.471 (0.048)	0.161 (0.054)	5
7:55:32.13	−24:14:44.8	12.990 (0.024)	0.282 (0.028)	1.249 (0.056)	12.960 (0.033)	0.084 (0.033)	−0.072 (0.035)	141
7:55:32.63	−24:14:08.3	14.762 (0.028)	0.627 (0.049)	1.123 (0.063)	14.604 (0.041)	0.419 (0.041)	0.122 (0.042)	121
7:55:33.46	−24:18:06.4	15.454 (0.050)	0.554 (0.064)	1.176 (0.075)	15.274 (0.054)	0.371 (0.054)	0.124 (0.065)	249
7:55:33.56	−24:18:21.7	12.936 (0.038)	1.683 (0.043)	3.603 (0.080)	12.261 (0.044)	1.440 (0.044)	0.666 (0.056)	260

[a]Values in parentheses are 1-σ random errors, including uncertainty of nightly fit to standards.

[b]Equinox J2000.

Table 3. NGC 2482 Cross-Identifications

ID_M[a]	ID_K[b]	Luminosity Class[c]
16	256	V
17	241/239	V
18	242	n
19	229	V
20	220/218	V
21	197	n
22	187	V
23	166	III
24	189	V
25	200	V
26	206	III
27	177	V
29	112	V
30	108	III
32	57	n
33	94	V
34	85	n
35	143	n
36	208	V

[a]ID in Moffat & Vogt (1975).

[b]ID in Table 2 of this paper.

[c]V = main sequence; III = giant; n = non-cluster member. From Moffat & Vogt (1975). Two of their stars (17 and 20) actually are comprised of two components. Their star number 35 is erroneously designated a non-member.

Table 4. Derived Results[a]

Cluster	log t (yrs)	D(pc)	E($B-V$)	R_V[b]	Z	[Fe/H][c]
AH03 J0748−26.9	7.80 (0.24)	4440 (353)	0.390 (0.025)	2.715 (0.263)	0.015 (0.006)	−0.10 (+0.15, −0.22)
NGC 2482	8.65 (0.09)	1194 (112)	0.094 (0.040)	...	0.015 (0.005)	−0.10 (+0.13, −0.18)
NGC 2482[d]	8.57 (0.09)	1349 (117)	0.086 (0.029)	...	0.022 (0.006)	+0.06 (+0.10, −0.14)
Ruprecht 42	8.60 (0.13)	5457 (418)	0.388 (0.061)	4.059 (0.875)	0.009 (0.003)	−0.33 (+0.13, −0.17)
Ruprecht 153	8.65 (0.17)	1848 (157)	0.206 (0.042)	4.111 (0.605)	0.024 (0.006)	+0.10 (+0.10, −0.13)
Ruprecht 154	9.35 (0.28)	1783 (175)	0.087 (0.024)	...	0.027 (0.004)	+0.15 (+0.06, −0.07)
Ruprecht 51	9.00 (0.07)	2514 (245)	0.189 (0.041)	3.415 (0.684)	0.021 (0.005)	+0.04 (+0.09, −0.12)

[a]Values in parentheses are 1-σ error bars. Except where noted, the results are derived from PSF photometry.

[b]If the color excess is less than 0.1 mag, we do not derive R_V.

[c][Fe/H] = $\log(Z/Z_\odot)$. The solar metallicity is taken to be 0.019.

[d]Results from aperture photometry.

Table 5. Exposure Times and Seeing[a]

Cluster	UT Date	t_u	s_U	t_B	s_B	t_V	s_V	t_g	s_g
NGC 2482	010612	24	2.7	3	2.6	3	2.4	3	2.2
	122112			150	3.3	120	3.4		
Ruprecht 51	123113	120	2.8	120	2.6	90	2.6	40	2.5
				20	2.4	6	2.4	6	2.5
AH03 J0748−26.9	010114	100	2.9	70	3.2	50	2.8		
		30	3.0	7	2.5	7	2.7	7	3.2
Ruprecht 42	010114	100	2.7	50	3.1	40	2.8	30	2.4
				5	2.9	5	2.4	5	2.4
Ruprecht 153	010314	120	3.1	60	3.2	40	3.1	25	3.0
		30	3.1	5	3.2	5	2.7	5	2.8
Ruprecht 154	010414	120	3.0	60	3.2	60	3.0	25	2.9
		30	3.2	5	3.1	5	2.9	5	2.7

[a]The UT date is in MMDDYY format. The nominal exposure times are given in seconds. The seeing (FWHM) is measured in pixels, where 1 px = 0.435 arc seconds. Nominal 3 second r and i exposures were also taken on 6 January 2012. The seeing was 2.2 and 1.9 px, respectively, for those exposures.

Table 6. Photometric Transformation Parameters from Standard Stars[a]

UT Date	Index	Extinction Term	Color Term	Zero Point	RMS
010612	V	0.12	−0.052 (0.015)	−2.903 (0.012)	± 0.010
	B	0.25	+0.042 (0.013)	−2.867 (0.010)	± 0.017
	$u' - g'$	0.43	1.004 (0.020)	−1.605 (0.073)	± 0.052
	r'	0.09	+0.008 (0.014)	−2.471 (0.007)	± 0.015
	$g' - r'$	0.04	0.961 (0.014)	0.237 (0.008)	± 0.016
	$r' - i'$	0.025	0.945 (0.019)	0.383 (0.005)	± 0.010
122112	V	0.105 (0.026)	−0.059 (0.016)	−3.086 (0.033)	± 0.022
	B	0.197 (0.030)	+0.063 (0.018)	−3.106 (0.038)	± 0.024
123113	V	0.103 (0.015)	−0.089 (0.011)	−1.310 (0.021)	± 0.019
	B	0.238 (0.015)	+0.077 (0.011)	−1.289 (0.021)	± 0.019
	$u' - g'$	0.271 (0.059)	1.000 (0.018)	−1.956 (0.096)	± 0.041
010114	V	0.146 (0.018)	−0.091 (0.009)	−1.253 (0.025)	± 0.015
	B	0.259 (0.019)	+0.083 (0.009)	−1.263 (0.026)	± 0.015
	$u' - g'$	0.350 (0.057)	1.003 (0.015)	−1.868 (0.107)	± 0.037
010314	V	0.14	−0.104 (0.012)	−1.257 (0.007)	± 0.017
	B	0.24	+0.064 (0.013)	−1.289 (0.008)	± 0.020
	$u' - g'$	0.311	1.002 (0.021)	−1.916 (0.077)	± 0.051
010414	V	0.108	−0.095 (0.008)	−1.340 (0.008)	± 0.020
	B	0.218	+0.073 (0.018)	−1.365 (0.010)	± 0.023
	$u' - g'$	0.311	1.035 (0.014)	−2.032 (0.047)	± 0.026

[a]UT date is in MMDDYY format. Extinction terms are measured in magnitudes per airmass. If no error bars are given, these are assumed values; on these nights all objects were observed over a small range of airmass. The B, V, and r' color terms scale instrumental $b - v$, $b - v$, and $g - r$ instrumental colors, respectively. Only aperture photometry was done with imagery of 21 December 2012. All other zeropoints refer to PSF photometry.

Fig. 1.— r' vs. $g' - r'$ color-magnitude diagram of 114 stars in the field of NGC 2482. Obvious non-members are plotted as red squares.

Fig. 2.— Color-color and color-magnitude magnitude diagrams of NGC 2482. In each panel the zero age main sequence is represented by a dashed line. The solid line is the best fit isochrone. The red dotted lines correspond to isochrones based on the parameters given by Kharchenko et al. (2013). The likelihood of a star being a cluster member is color coded according to the key in the top right-hand panel, and is also proportional to the size of the points.

Fig. 3.— A finder for the NGC 2482 stars discussed in this paper. North is up, east to the left. The X marks the nominal location of the cluster center from Dias et al. (2002). We sorted the stars according to the V-band photometry, and binned the data from 10.0 to 10.99, 11.00 to 11.99 etc. The sizes of the points in this figure decrease with the brightness of the stars. As in Fig. 1, likely cluster members are plotted as round dots; likely giant stars at some other distance are plotted as red squares. Stars 17 and 20 of Moffat & Vogt (1975) have close companions visible in the CCD images; these companions are plotted as cyan-colored dots. Star 166 is a bona fide giant in the cluster. Stars 108 and 206 are also past the turnoff point.

Fig. 4.— Comparison of photometry of NGC 2482 done with aperture photometry and with PSF photometry. For the top two panels we used BV aperture photometry of 6 January 2012 (short exposures) for stars brighter than $V \approx 13.2$ and aperture photometry of 21 December 2012 (long exposures) for stars fainter than $V \approx 13.2$. Sloan u-band and g-band images were only taken on 6 January 2012. This figure illustrates the consistency of the photometry taken with short and long exposure times on two different nights, and the consistency of photometry derived using instrumental magnitudes obtained with two different methods.

Fig. 5.— Comparison of the density maps of our six clusters. For Ruprecht 153 the map was obtained with a Gaussian kernel of $\sigma = 2.5'$. For the other clusters we used a kernal of $1'$.

Fig. 6.— Histograms of relative likelihood of stellar age, distance, and color excess for the presumed cluster Ruprecht 154. The upper left and lower right panels suggest that there are two populations of stars along this line of sight.

Fig. 7.— Same as Fig. 2, but for AH03 J0748−26.9.

Fig. 8.— Same as Fig. 2, but for Ruprecht 42.

Fig. 9.— Same as Fig. 2, but for Ruprecht 51.

Fig. 10.— Same as Fig. 2, but for Ruprecht 153.

Fig. 11.— Same as Fig. 2, but for Ruprecht 154.

Fig. 12.— Metallicity [Fe/H] of clusters vs. cluster distance from Galactic Center (in kpc). The Sun's distance is taken to be 8.0 kpc from the Galactic Center. The dashed lines are based on Lépine et al. (2011).

Fig. 13.— Locations of clusters in the Galactic X-Y plane. Here we adopt the convention that +X is in the direction of Galactic longitude 90°. +Y is in the direction of Galactic longitude 180°. Small colored dots: from Dias et al. (2002). Large colored dots: data of this paper. Large grey dot: position of the Sun. The points are color coded by age. The data are binned by 1.0 in log t (in years). From the youngest clusters to the oldest the color coding is as follows: blue (log t from 6.0 to 7.0^-), green (7.0 to 8.0^-), yellow (8.0 to 9.0^-), and red (9.0 to 10.0). The approximate boundaries of the Orion Spur and the Perseus arm are from Fig. 16 of Churchwell, et al. (2009).

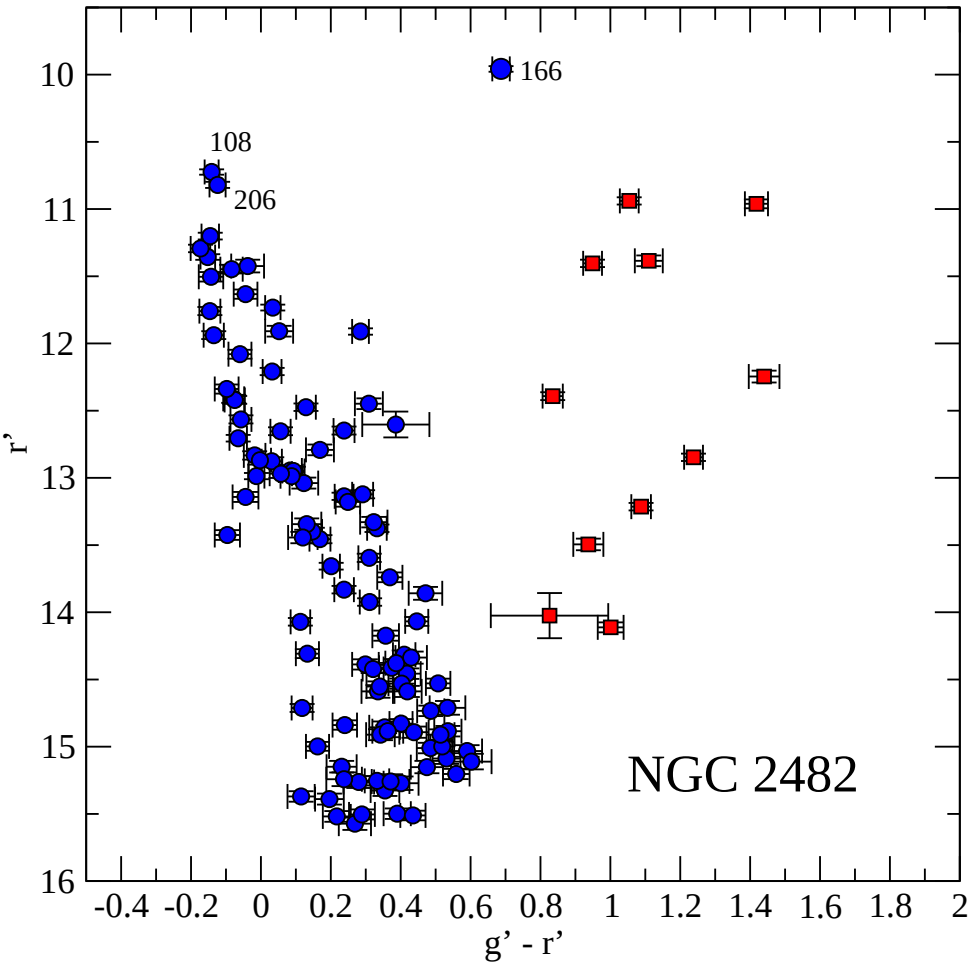
166
108
206
NGC 2482
r'
g' - r'
10
11
12
13
14
15
16
-0.4
-0.2
0
0.2
0.4
0.6
0.8
1
1.2
1.4
1.6
1.8
2

Fig. 1.

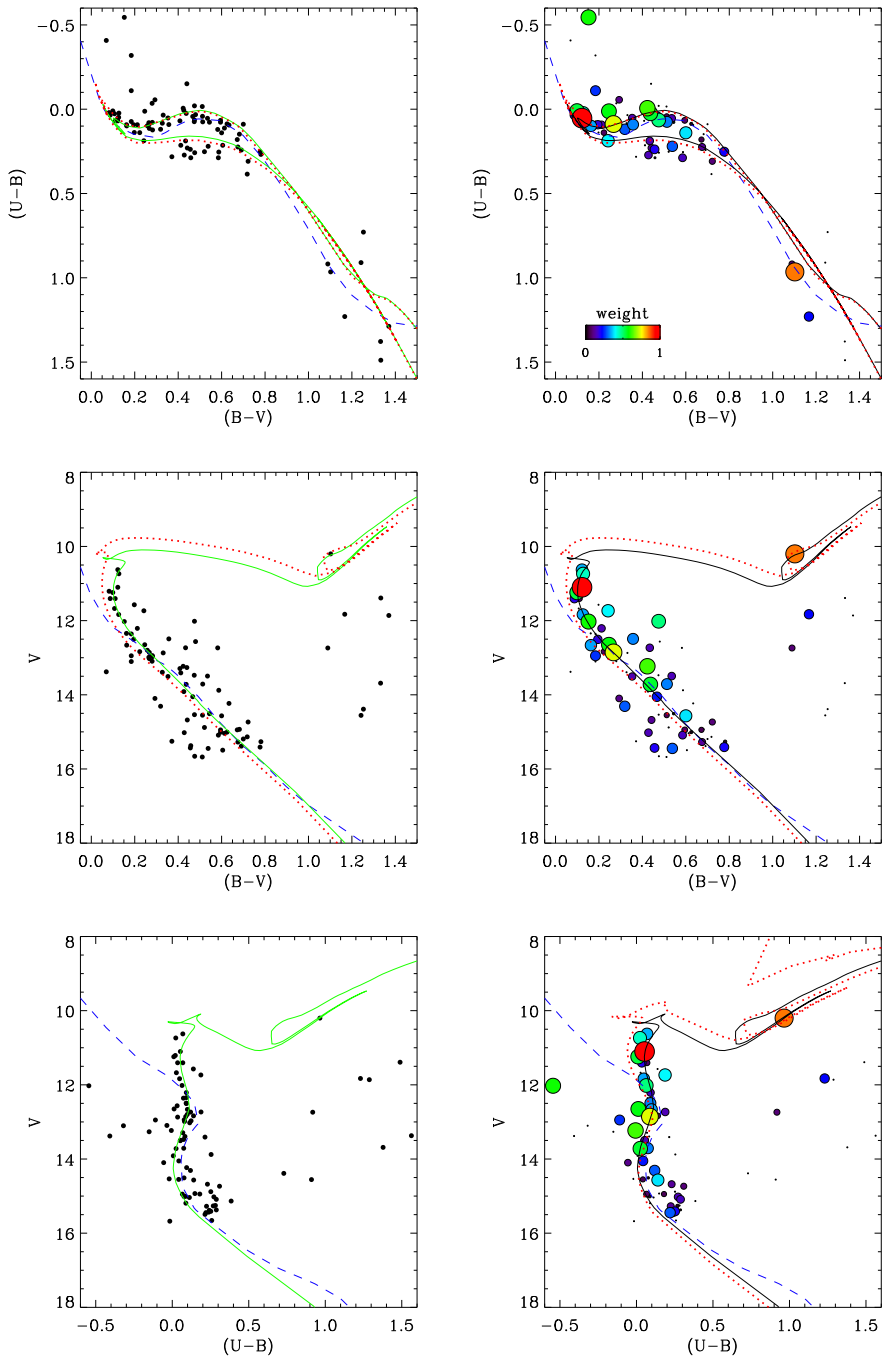

Fig. 2.

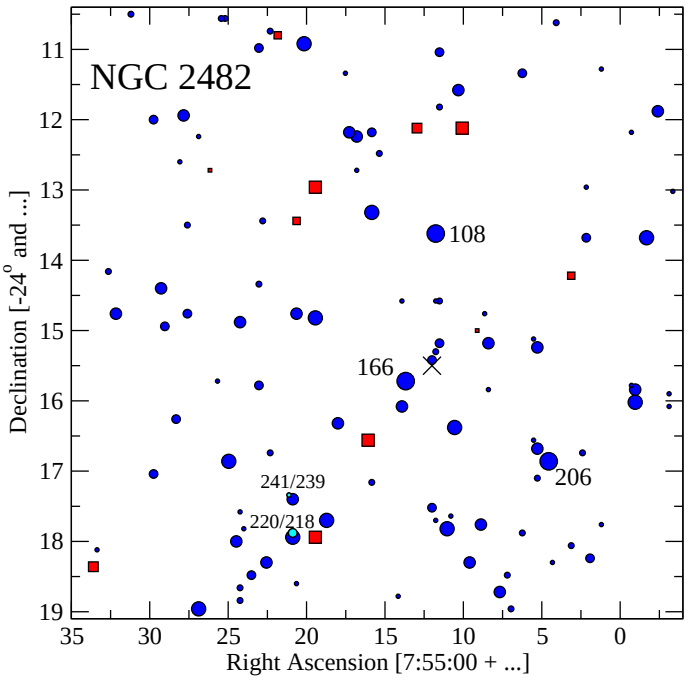
NGC 2482
108
166
206
241/239
220/218
Declination [-24° and ...]
Right Ascension [7:55:00 + ...]
11
12
13
14
15
16
17
18
19
35
30
25
20
15
10
5
0

Fig. 3.

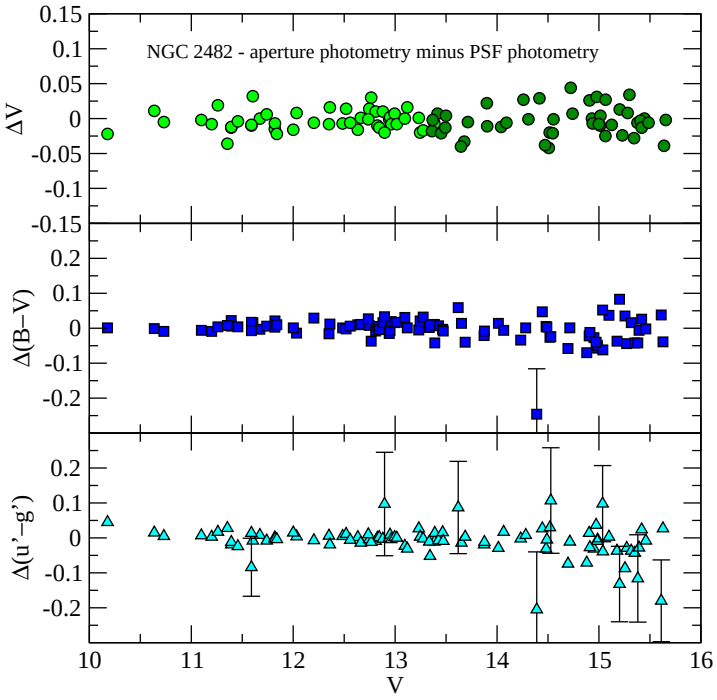
NGC 2482 - aperture photometry minus PSF photometry
ΔV
Δ(B−V)
Δ(u'−g')
V
0.15
0.1
0.05
0
-0.05
-0.1
-0.15
0.2
0.1
0
-0.1
-0.2
10
11
12
13
14
15
16

Fig. 4.

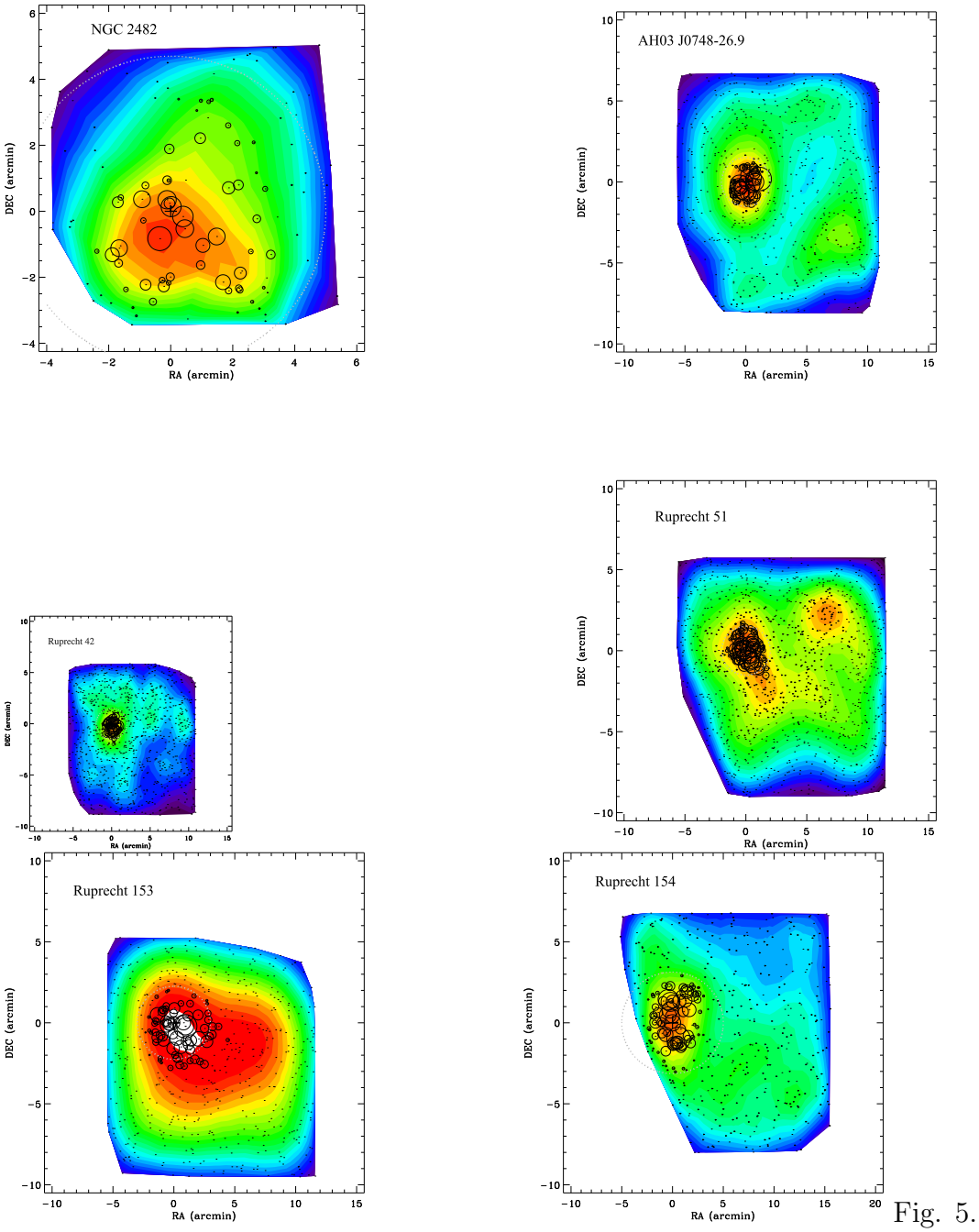
NGC 2482
AH03 J0748-26.9
Ruprecht 51
Ruprecht 42
Ruprecht 153
Ruprecht 154
DEC (arcmin)
RA (arcmin)

Fig. 5.

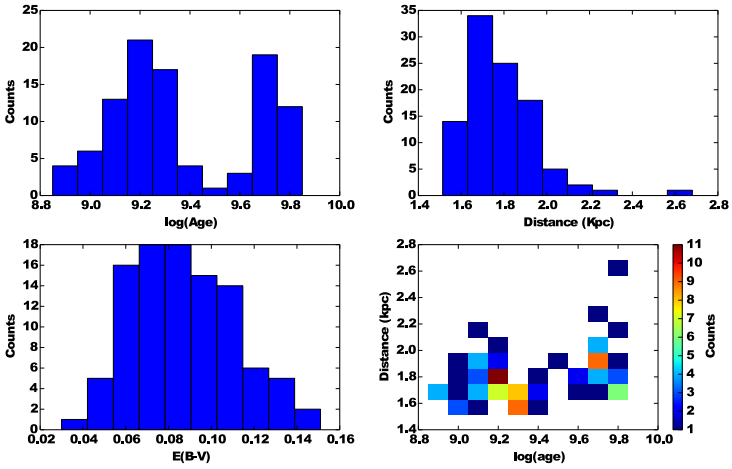
Counts
log(Age)
Counts
Distance (Kpc)
Counts
E(B-V)
Distance (kpc)
log(age)
Counts

Fig. 6.

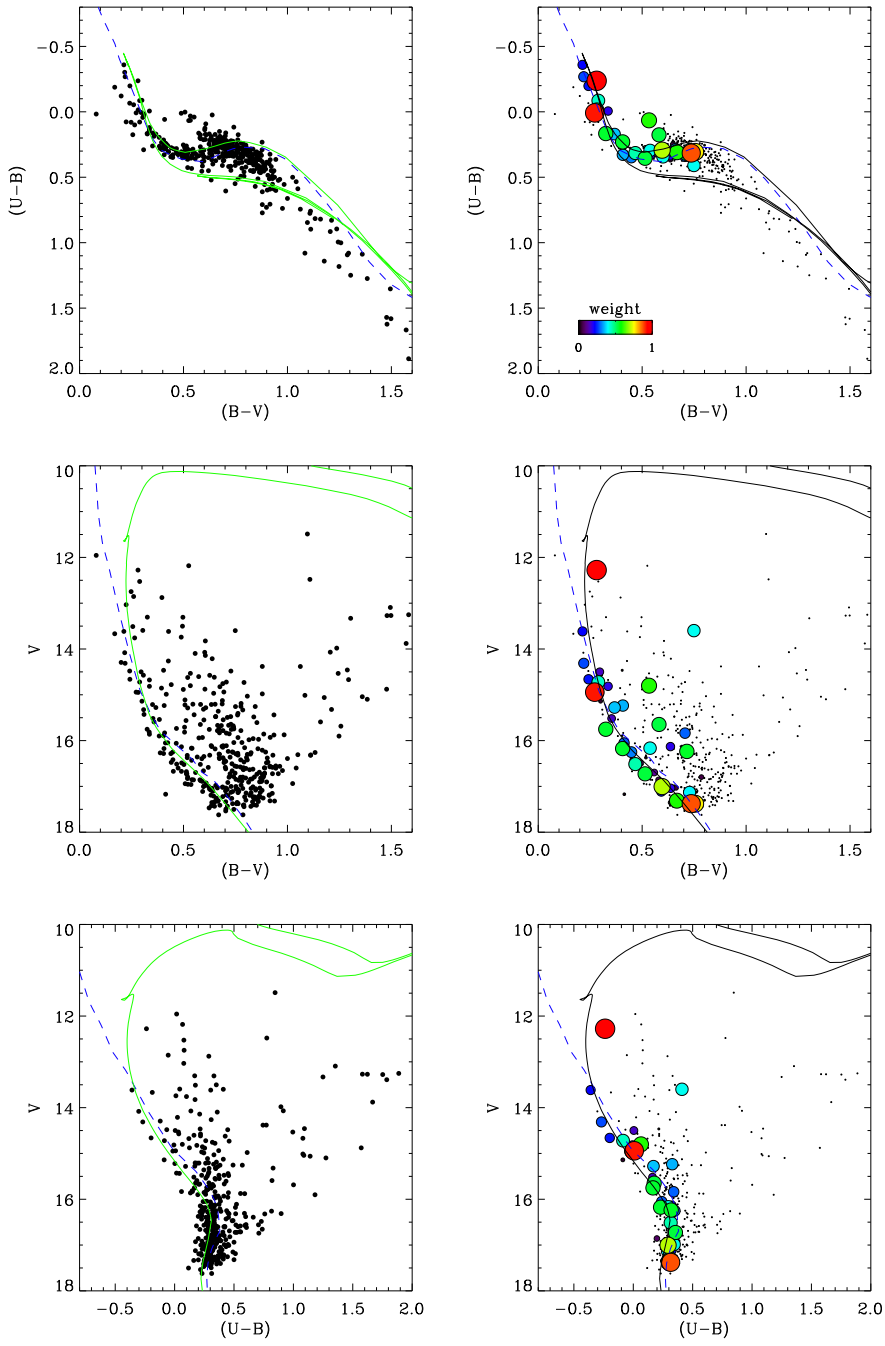

Fig. 7.

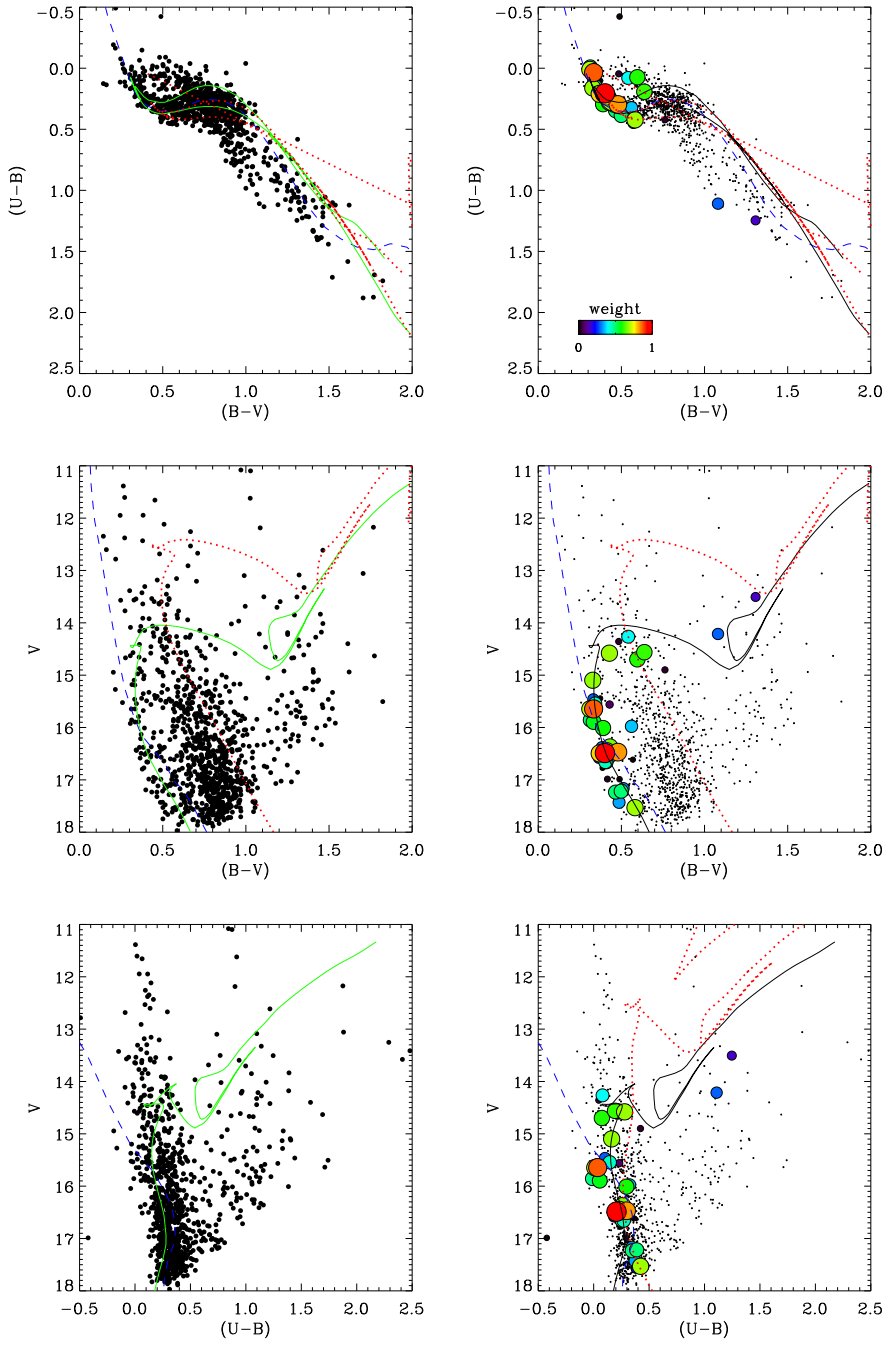

Fig. 8.

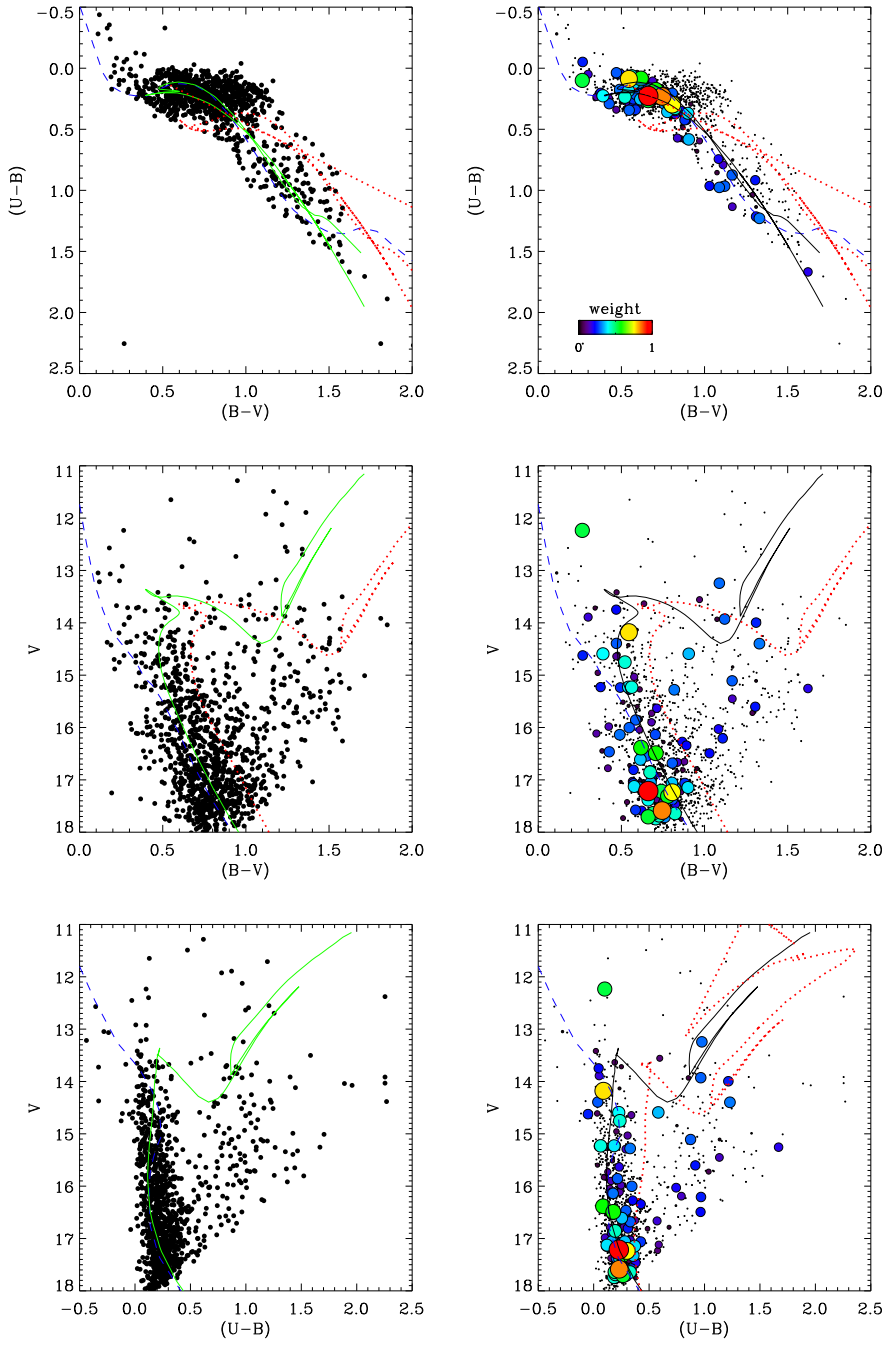

Fig. 9.

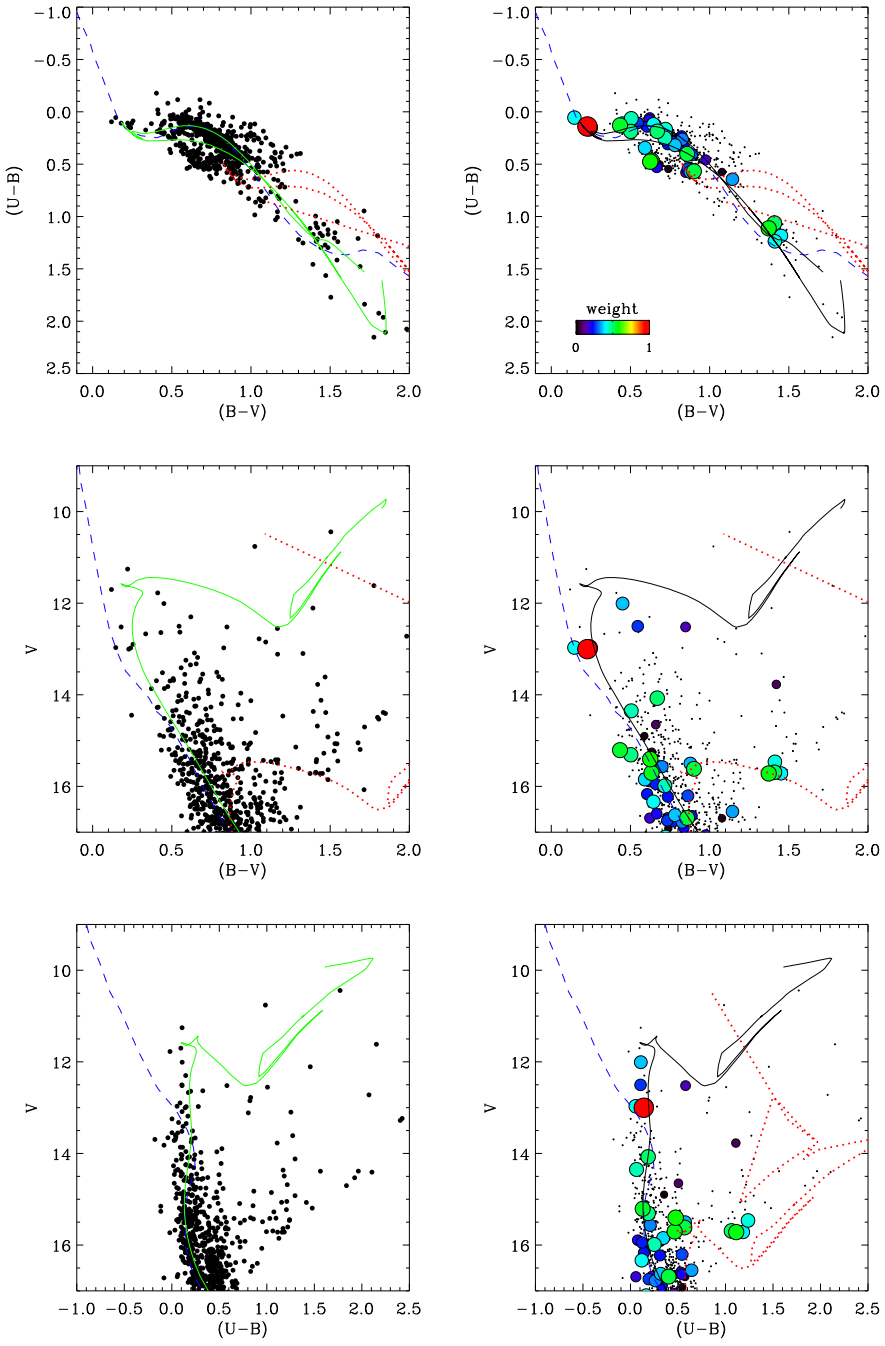

Fig. 10.

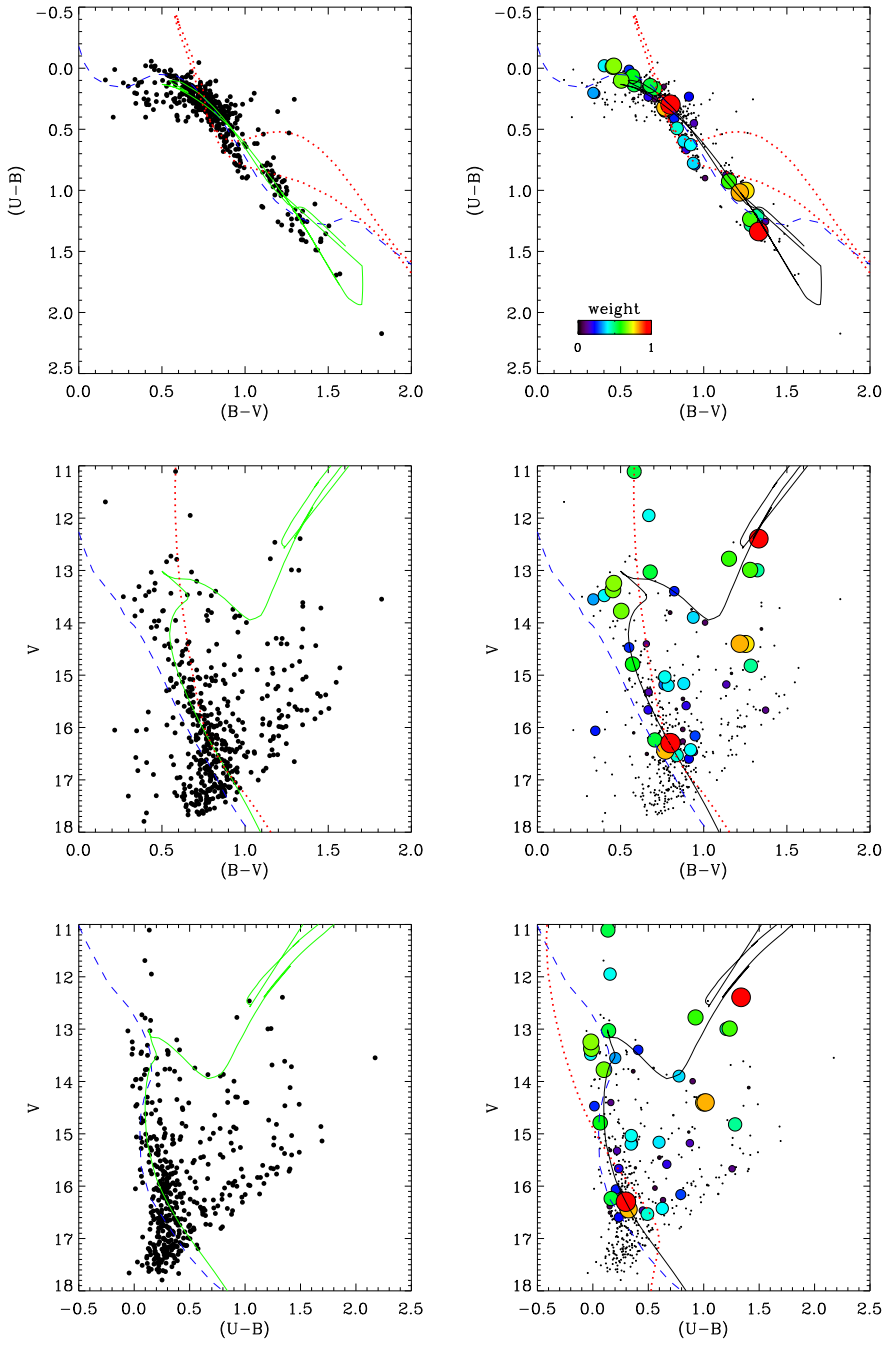

Fig. 11.

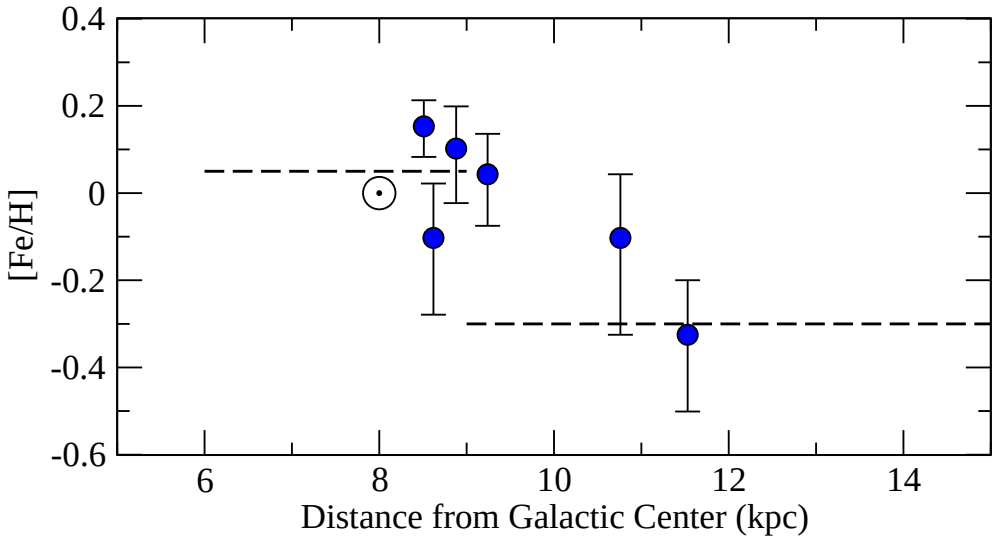
0.4
0.2
0
-0.2
-0.4
-0.6
[Fe/H]
6
8
10
12
14
Distance from Galactic Center (kpc)

Fig. 12.

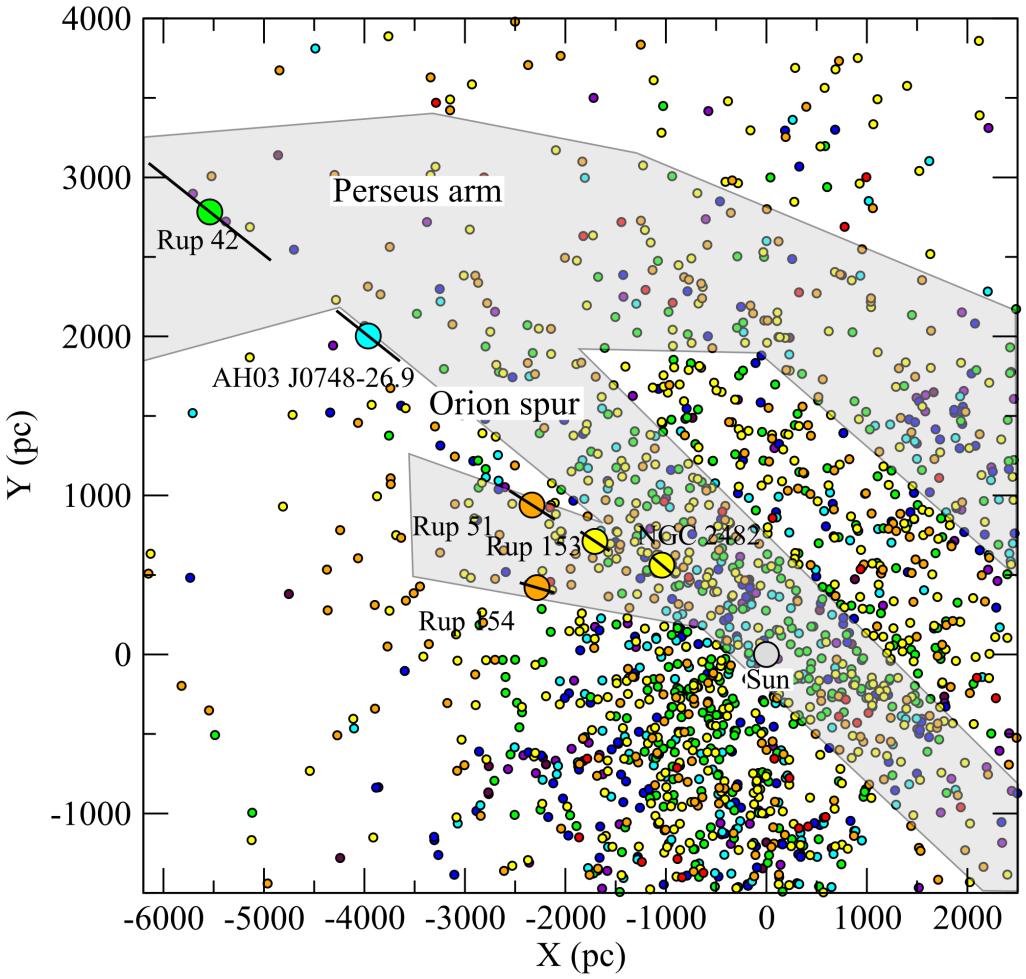
Perseus arm
Rup 42
AH03 J0748-26.9
Orion spur
Rup 51
Rup 153
NGC 2482
Rup 154
Sun
Y (pc)
X (pc)
4000
3000
2000
1000
0
-1000
-6000
-5000
-4000
-3000
-2000
-1000
0
1000
2000

Fig. 13.